

Stop 1. Bastendorff Beach

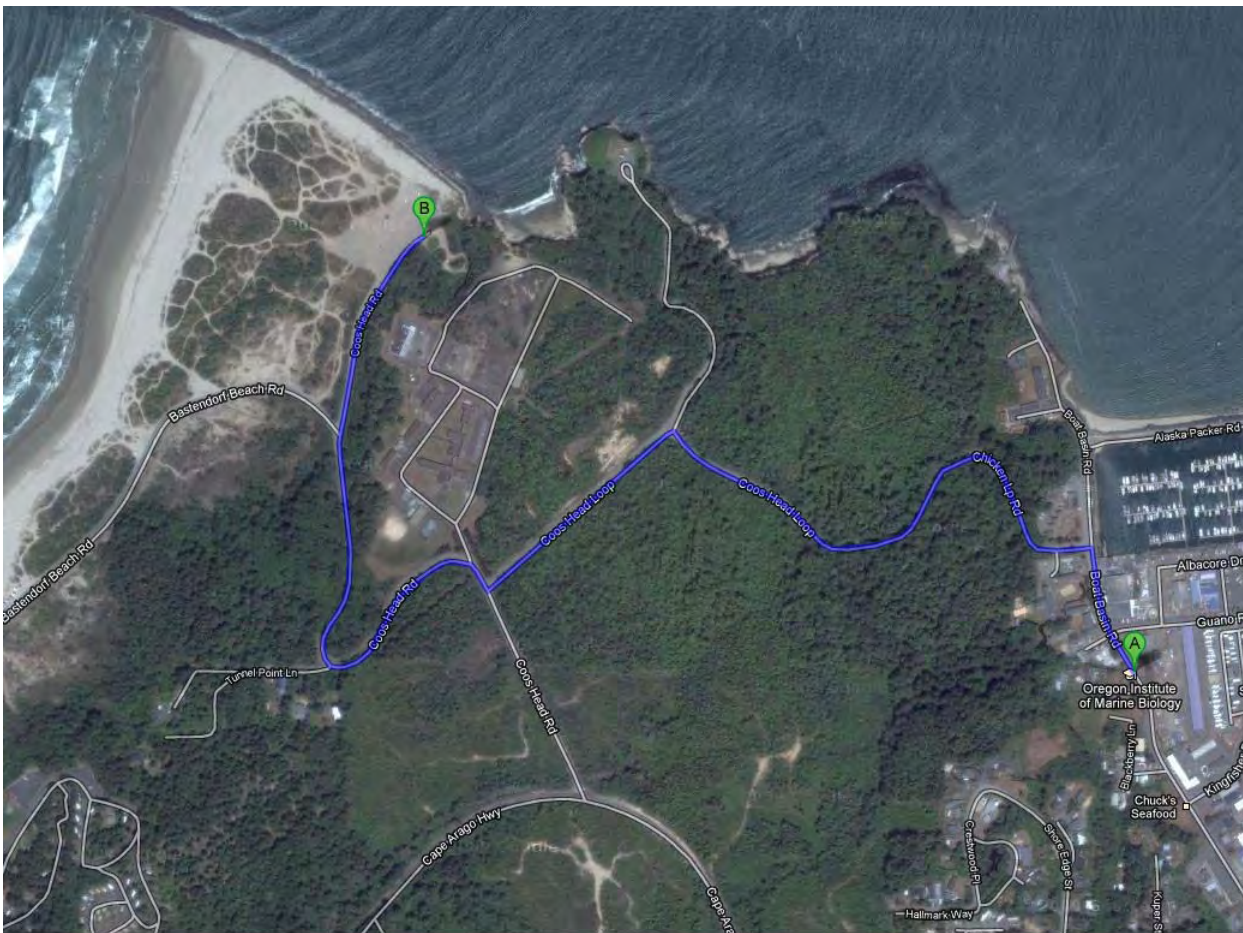


Figure 1-1. Navigation

Leaving OIMB, our first stop is Bastendorff Beach, a short drive over Coos Head.

Oregon Beach dynamics

The Oregon Coast is highly active, with one of the most energetic wave climates (Figure 1-2) in the world, and all of that energy pushes a lot of sand around. We all learned about longshore drift in Geo 101, but the pattern in Oregon is fundamentally different. Oregon's coast is broken into a series of "pocket beach" littoral cells, long stretches of dune or bluff-backed beach bounded by rocky headlands that extend into water that is deep enough to block sediment transport around the ends of the headlands. There are also large differences in the direction and energy of summer versus winter waves (Figure 1-3); highly energetic winter waves erode the beaches and move sand offshore to form sand bars, while gentler summer waves restore the sand to the beaches. Within each cell, sand also moves north or south depending on the prevailing wave directions and in response to climate events such as El Niño's. Here at Bastendorff beach we see evidence for this intra-cell movement in the form of dramatic accretion of the beach since the construction of the south jetty in the early 1900's. The beach rapidly accreted (Figure 1-3) until about 1967, and has reached some state of equilibrium since then. The abandoned sea cliff is now hidden behind the forest of shore pines, but is clearly visible on lidar. Also typical of the Oregon Coast, the backshore at Bastendorff beach has been rapidly and effectively stabilized by

European dune grass, a non-native species that have substantially changed dune characteristics in the last century.

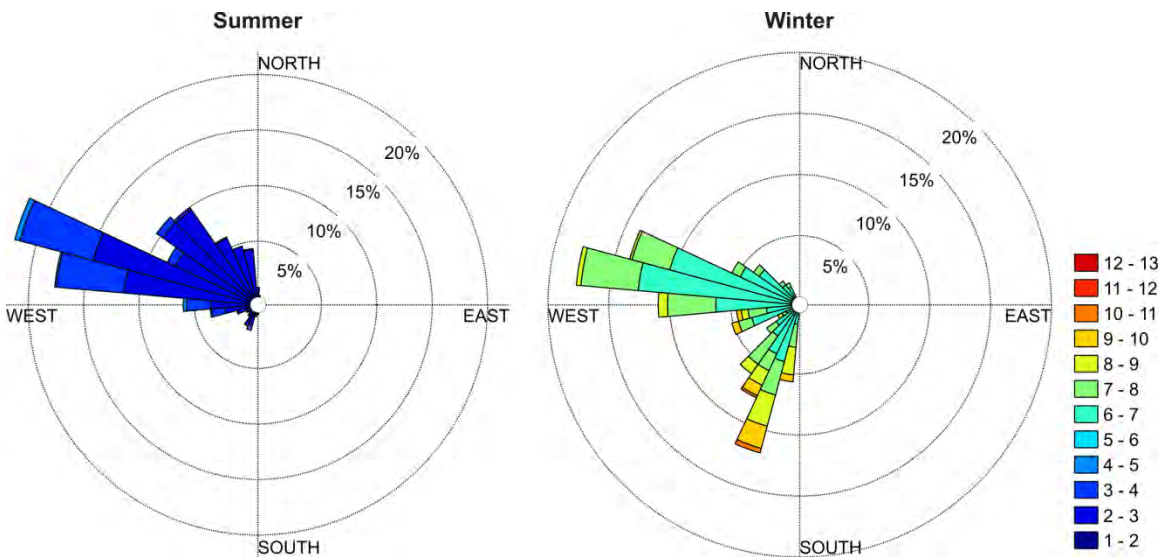
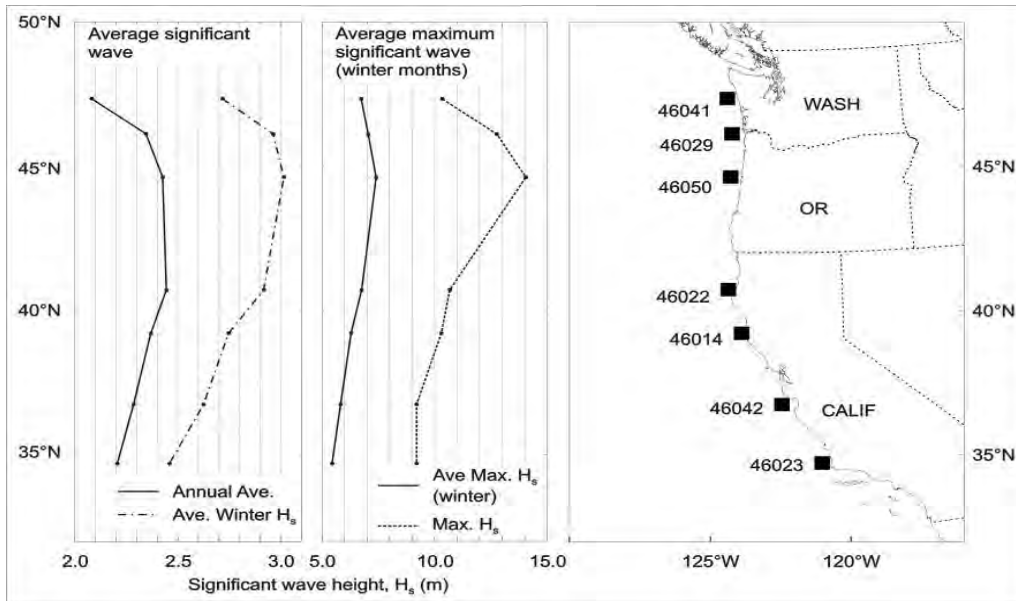


Figure 1-2. Top: Wave heights on the US west coast. Bottom: Winter vs summer wave directions offshore from the central Oregon coast. Colored scale indicates the wave height in meters.

The introduction of European beach grass, (*Ammophila arenaria*) in the early 1900s for the purposes of dune stabilization and its eventual proliferation along the coast, has without doubt single-handedly transformed the character of the coast, particularly since the late 1930s. For example, the first state-wide aerial photographic survey of the coast in 1939 clearly shows that the majority of the dunes and barrier spits on the coast were completely devoid of vegetation. At that time, the expanse of low lying hummocky dunes allowed sand to be transported significant distances inland, where the dunes piled up against marine terraces where present, or inundated forest communities. With the introduction of European beach grass, particularly in the late 1960s and early 1970s when extensive dune planting programs took place, the dunes and barrier spits have subsequently become stabilized, building foredunes that now range in height from 10- 16 m.

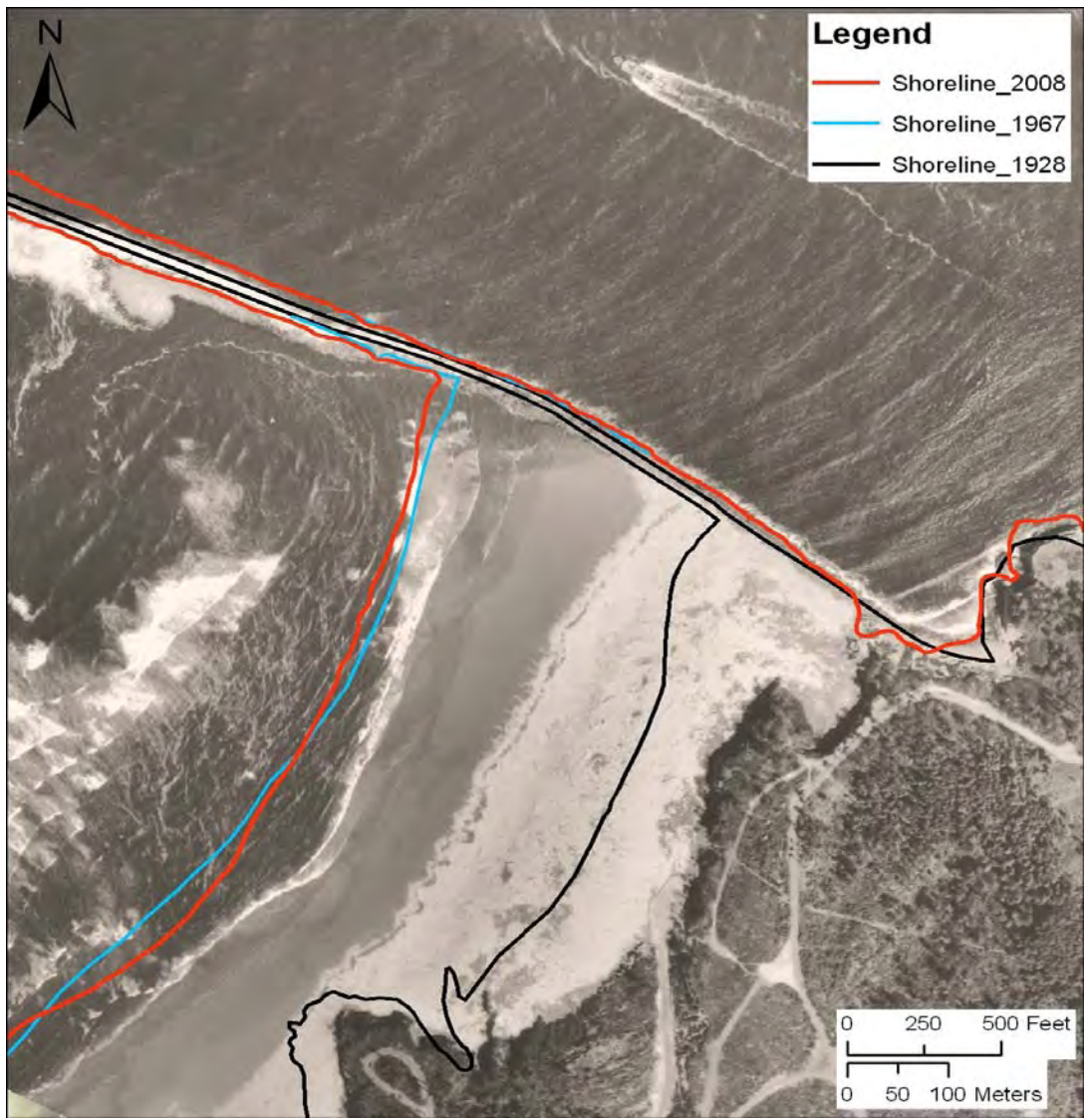


Figure 1-3. Historic shorelines at Bastendorf Beach, photo is from 1939.

Periodic extreme storms, such as occur during El Nino or La Nina events can cause dramatic erosion within littoral cells, and in some cases appear to actually move sand out of the cell, or into water so deep that summer waves cannot return it. Understanding beach erosion and dynamics therefore requires detailed quantitative data, so that one can begin to sort out the cyclic changes from the permanent changes. Jonathan Allan, DOGAMI’s coastal geomorphologist, has pioneered this effort, using serial lidar and repeat RTK-GPS surveys to track beach changes. There are several iterations of coastal lidar currently available, and although the earlier data are much lower resolution and accuracy than current Oregon Lidar Consortium data, they are sufficiently accurate in the relatively flat and well-exposed beach areas to allow for quantitative comparison. However, beach changes take place at far shorter intervals than the time between lidar flights, and weather precludes lidar collection during most of the winter, when changes are greatest. To get around this, Jon has established a series of monitoring profiles up and down the coast where he does repeat RTK-GPS surveys with sufficient accuracy to detect changes in elevation of 4-5 cm, a small fraction of the typical 1-3m seasonal change in beach elevation.

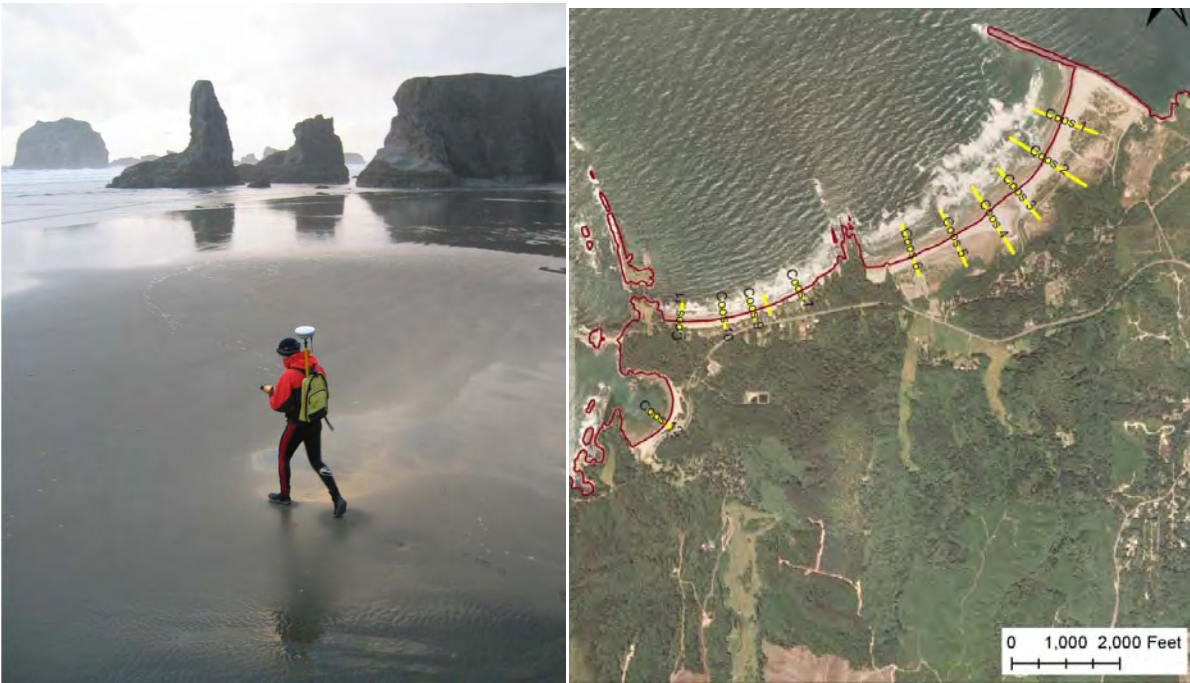


Figure 1-4. RTK-GPS beach profiling and location of transects at Bastendorf Beach. Data for these sites and many others are available at: <http://www.nanoos.org/nvs/nvs.php?section=NVS-Products-Beaches-Mapping>.

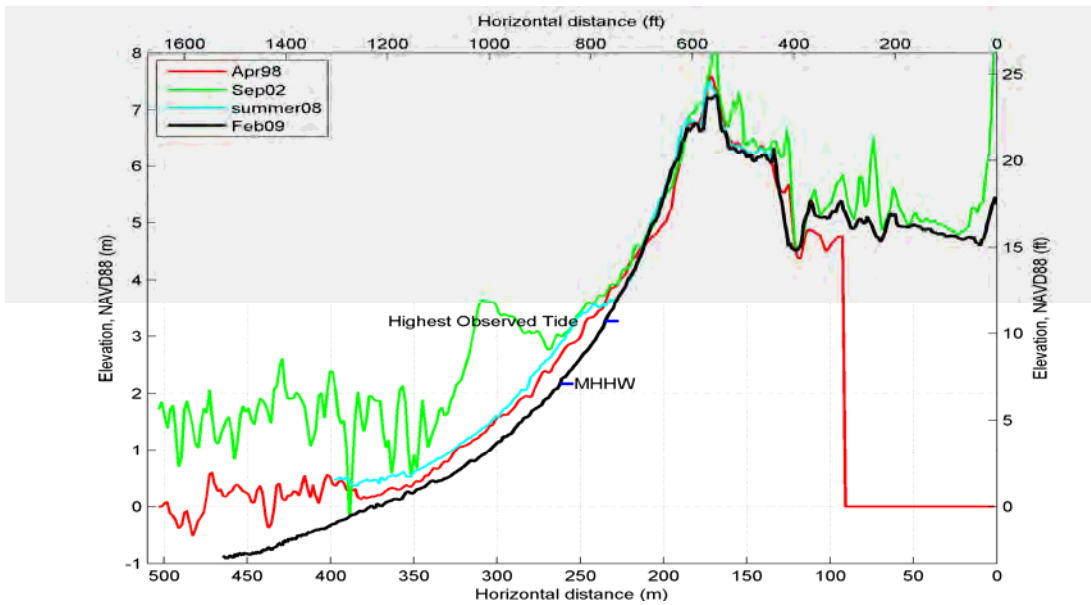


Figure 1-5: The Coos 2 profile site indicating the generally low backshore elevations that suggest that the beach probably prograded rapidly seaward following jetty construction, while the high contemporary foredune indicates that the shoreline has stabilized.

For those interested in rocks, the shoreline behind the beach is composed of a sequence of steeply E-dipping Eocene and Oligocene marine sedimentary rocks, overlain just at our stop by Miocene marine mudstone with a significant angular unconformity.

Stop 2: Shore Acres State Park



Figure 2-1. Navigation

Leaving Bastendorf Beach, Stop 2 at Shore Acres State Park is a short drive down the Cape Arago Highway. There is a \$5 per car day use/entry fee required at Shore Acres.

Shore Acres is an iconic bit of Oregon coastal scenery. Thick sandstone beds of the lower Coaledo Formation dip moderately inland, forming beautifully sculpted ramparts against which huge waves crash (Figure 2-2). The broad flat surface on which the park is located is the lowest of a well-defined sequence of marine terraces that are present in the Coos Head-Cape Arago region. As we all remember from Geomorph 101, marine terraces form during times of stable or slowly rising sea level, as waves erode the shoreline, carving a submarine wave-cut platform as erosion progresses inland. The platforms end at the paleo-sea cliff commonly referred to as the shoreline angle or backedge, and are covered with nearshore marine sediments of varying thickness. As sea level cycled during the Pleistocene, tectonically rising coasts preserved a stair step sequence of terraces like those we see here. These terraces were dated by McInnelly and Kelsey (1990) and then mapped in detail by Madin, McInnelly and Kelsey (1995). The terraces are:

- Whisky Run (80 ka, Stage 5a)
- Pioneer (105 ka, Stage 5c)
- Seven Devils (125 ka Stage 5 d or e?)
- Metcalf (200-250 ka, Stage 7)

An older Arago terrace may or may not exist. On the lidar image (Figure 2-3) we can clearly see the flat Whiskey Run surface (Qwr, generally violet and blue elevation colors) and its well-defined backedge, the Pioneer Terrace (pale blue elevation tint) is quite dissected with little of the backedge preserved, as is the Seven Devils terrace (yellow elevation



Figure 2-2. Shore Acres Park, note people for scale.

tint), and the Metcalf terrace (brick red elevation tint) is even more deeply eroded (and tilted) and is largely preserved capping ridges

We are standing on the Whiskey Run terrace and all along the edge of the modern sea cliff you can see the exposed wave cut platform and the very thin terrace cover sediments. The marine terraces are rapidly formed planar surfaces that define sea level at a particular stage, so they are excellent markers for tectonic deformation. Figures 2-3 and 2-4 show a cross section of deformation through this area, as well as calculated uplift rates for the various terraces. Care must be taken to work with the wave-cut platform, not the terrace surface, because the thickness of the terrace cover sediments varies widely.

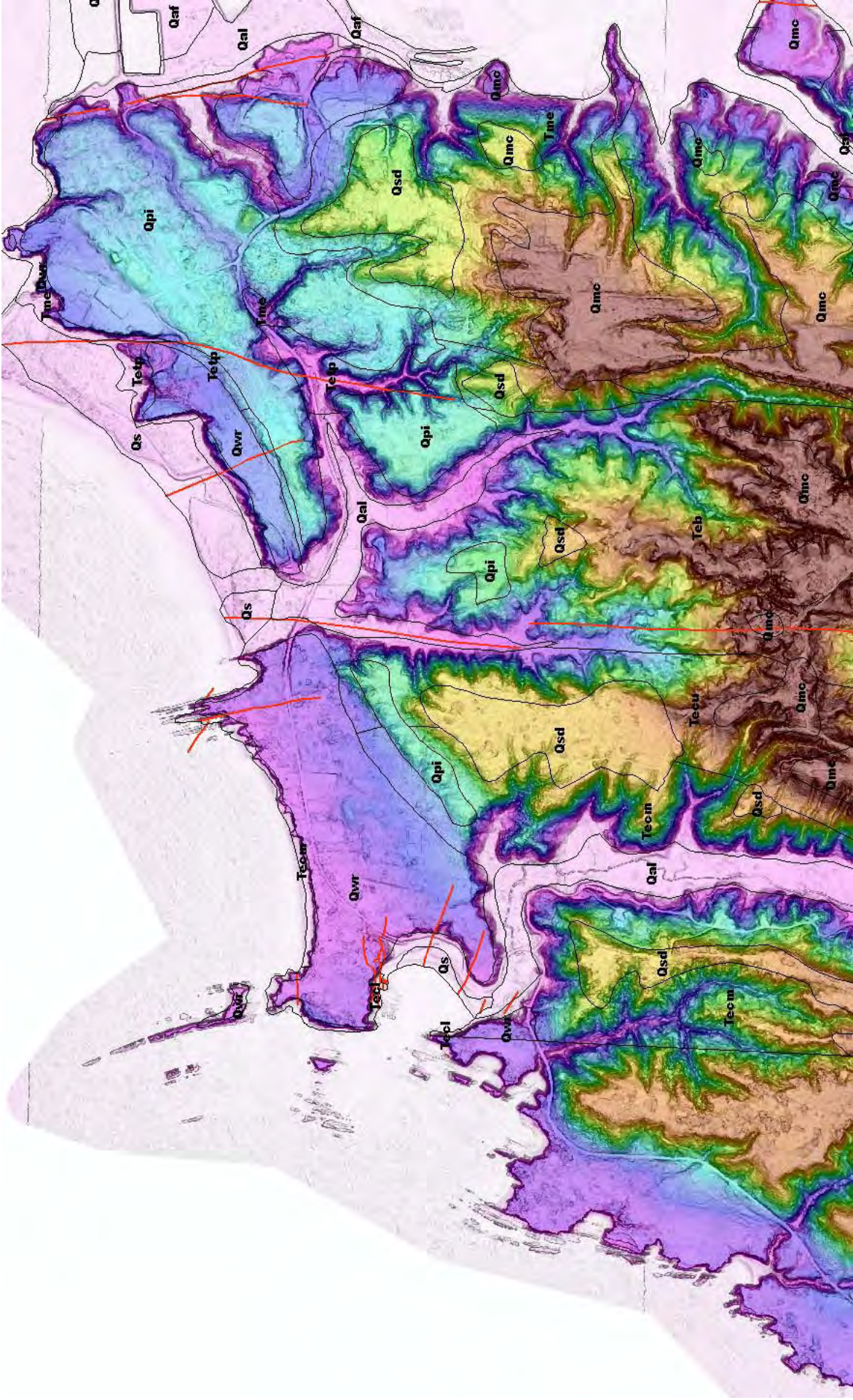


Figure 2-3. Lidar image (slopesshade and colored elevation gradient) and geologic map of Coos Head. Geologic units are Qaf, artificial fill; Qal, beach deposits; Qal, alluvium; Qvr, Whisky Run terrace; Qpi, Pioneer terrace; Qsd, Seven Devils terrace; Qmc, Metcalf terrace; Tme, Empire Formation; Totp, Tunnel Point Formation; Teb, Bastendorf Shale; Tecu, upper Coaledo Formation; Tecm, Middle Coaledo Formation; Tecl, lower Coaledo Formation.

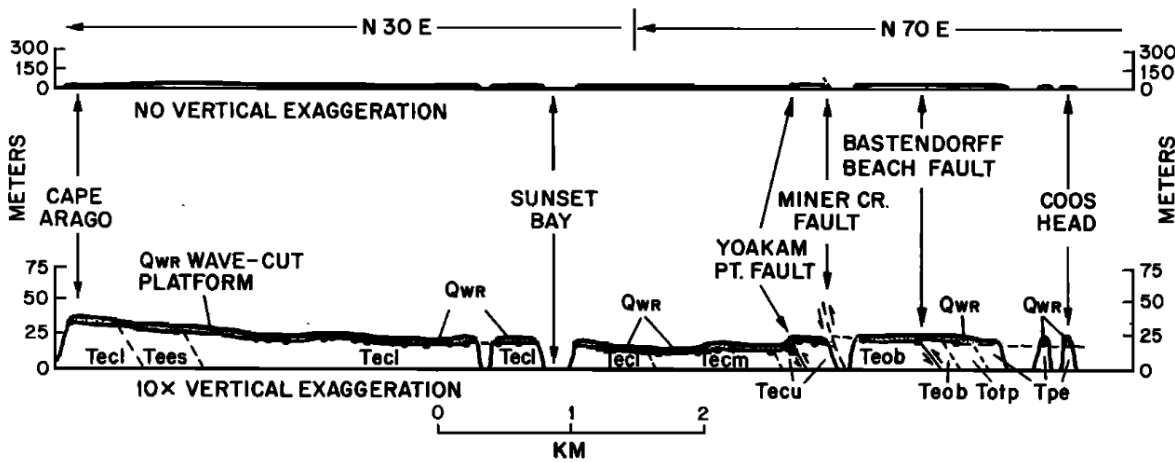


Fig. 7. Post-80 ka deformation of the Whisky Run wave-cut platform is illustrated in this coastwise transect from Cape Arago to Coos Head (view to northwest and north-northwest). Solid circles are altimeter survey locations. Data are projected onto a line that trends N30°E from Cape Arago to Sunset Bay, then N70°E to Coos Head. The gradual descent of the Whisky Run Wave-cut platform from Cape Arago to Coos Head is interrupted repeatedly by flexural-slip faults at Yoakam Point, Miner Creek, and Bastendorff Beach. Geologic units are same as previous figure.

Figure 2-4. Deformation of Whisky Run terrace between Cape Arago and Coos Head

TABLE 2. Marine Wave-Cut Platforms at Cape Arago: Ages, Uplift Rates, Tilt Rates, and Horizontal Strain Rates

Wave-Cut Platform	Estimated Age, ka	Maximum Elevation, ^a m	Shore-Normal Distance From Shoreline Angle, km	Original Gradient of Platform, m/km	Original Depth of Platform, m	Paleo-Sea Level, ^b m	Sea Level Model ^c	Maximum Uplift Rate, ^d m/kyr	Elevation of Shoreline Angle, m	Uplift Rate at Shoreline angle, m/kyr	Maximum Observed Tilt, ^e rad	Tilt Rate rad/yr	Horizontal Strain Rate, ^f yr ⁻¹
Whisky Run	80	35	0.2	20	4	-19 ± 5	NG	0.73 ± 0.07	31	0.63 ± 0.07	2.3 × 10 ⁻³	2.9 × 10 ⁻⁸	0.44 × 10 ⁻⁷
	80	35	0.2	40	8	-19 ± 5	NG	0.78 ± 0.07	31	0.63 ± 0.07			
	80	35	0.2	20	4	-5 ± 2	CA-JP	0.55 ± 0.03	31	0.45 ± 0.03			
	80	35	0.2	40	8	-5 ± 2	CA-JP	0.60 ± 0.03	31	0.45 ± 0.03			
Pioneer	105	68 ^g	0	NA	0	-9 ± 3	NG	0.73 ± 0.03	68	0.73 ± 0.03	5.7 × 10 ⁻³	5.4 × 10 ⁻⁸	0.83 × 10 ⁻⁷
	105	68 ^g	0	NA	0	-2	CA-JP	0.67	68	0.67			
Seven Devils ^h	125	100	0.2	20	4	+6	both	0.78?	98 ^g	0.74?	8.1 × 10 ⁻³ ?	6.5 × 10 ⁻⁸ ?	1.0 × 10 ⁻⁷ ?
	125	100	0.2	40	8	+6	both	0.82?	98 ^g	0.74?			
Metcalf ^h	200?	169	0	NA	0	B+2		0.84?	169	0.84?	17 × 10 ⁻³ ?	8.5 × 10 ⁻⁸	1.3 × 10 ⁻⁷ ?

^aFor Whisky Run and Seven Devils platforms, the maximum elevation near Cape Arago is 200 m seaward (westward) of the paleoshoreline angle. For Pioneer and Metcalf platforms the maximum elevation near Cape Arago is at the paleoshoreline angle. All platforms are landward tilted at Cape Arago.

^bRelative to present sea level.

^cNG, New Guinea model [Chappell and Shackleton, 1986]; CA-JP, California-Japan model [Machida, 1975; Muhs et al., 1988]; B, Bermuda data for 200 ka high stand [Harmon et al., 1983].

^dUncertainties for Whisky Run and Seven Devils wave-cut platforms: (1) paleo-sea level, (2) paleo-water depth during the 80 and 105 ka sea level high stands for the present point of maximum elevation.

^eFor all terrace platforms, tilt is measured from the vicinity of Cape Arago N60°E to the vicinity of South Slough. Tilts measured parallel to the N60°E down dip direction.

^fSee assumptions for derivation of strain rate in text.

^gElevation is extrapolated from known distance measured in downdip direction and using average platform tilt.

^hThe estimated ages of the Seven Devils and Metcalf platforms are minimum ages and not constrained by isotopic data. Therefore all calculated rates based on these ages are maximum rates and are queried because of the large uncertainties.

MCINNELLY AND KELSEY: TECTONIC DEFORMATION, COASTAL OREGON

Figure 2-5. Measured deformation rates for terraces between Cape Arago and Coos Head.

Note also that the offshore rocks here very clearly define the structure of the steeply dipping and folded marine strata. All along this stretch of coast, the geologic structure has a strong influence on the shape of the coastline, for instance Sunset Bay has formed where a series of scissor faults perpendicular to the bedding have weakened the resistant sandstone rips enough to allow wave erosion to penetrate inland and then spread where it encounters mudstone and siltstone.

Figure 2-6 shows a 2ft contour map of the Shore Acres area and the paleo sea cliff behind it. There are two large alluvial fans that emanate from very small gullies in the sea cliff, and are built out onto the Whisky Run terrace surface. George Priest from the DOGAMI Newport field office has been mapping the Oregon coast in detail for years, and he sees evidence that Western Oregon endured a much colder and wetter climate than today from shortly after the last high sea stand ~80,000 years ago until ~10,000 years ago. During much of this period sea level was ~200-400 feet lower than today with annual rainfall probably approaching that of southeast Alaska, hundreds of inches per year. Cascadia subduction zone earthquakes shook the region about every 500 years, sometimes occurring during winter when slopes

were least stable. As a result, numerous deep bedrock slides and debris flows covered most steep slopes. These old landslides and colluvial deposits now form a more or less continuous, semi-consolidated deposit in many areas. These unusual fans may be the result of that extremely wet and active period.

Finally, here is an opportunity to make a point about using lidar for geologic maps, and I can beat up on this map because it is mine (from 17 years ago). Compared to the lidar geomorphology, a few of the contacts in Figure 2-3 are pretty good, but most are off by tens of meters or more. I also completely missed the obvious extension of the Whisky Run terrace and backedge to the east of the fault that extends under Bastendorf Beach, and completely missed the landslide at the back of the beach, as well as two additional faults crossing the Whisky Run terrace near Sunset Bay. The moral of the story is that if you are making a geologic map, get lidar first, so future generations don't make fun of your work in field trip guides.

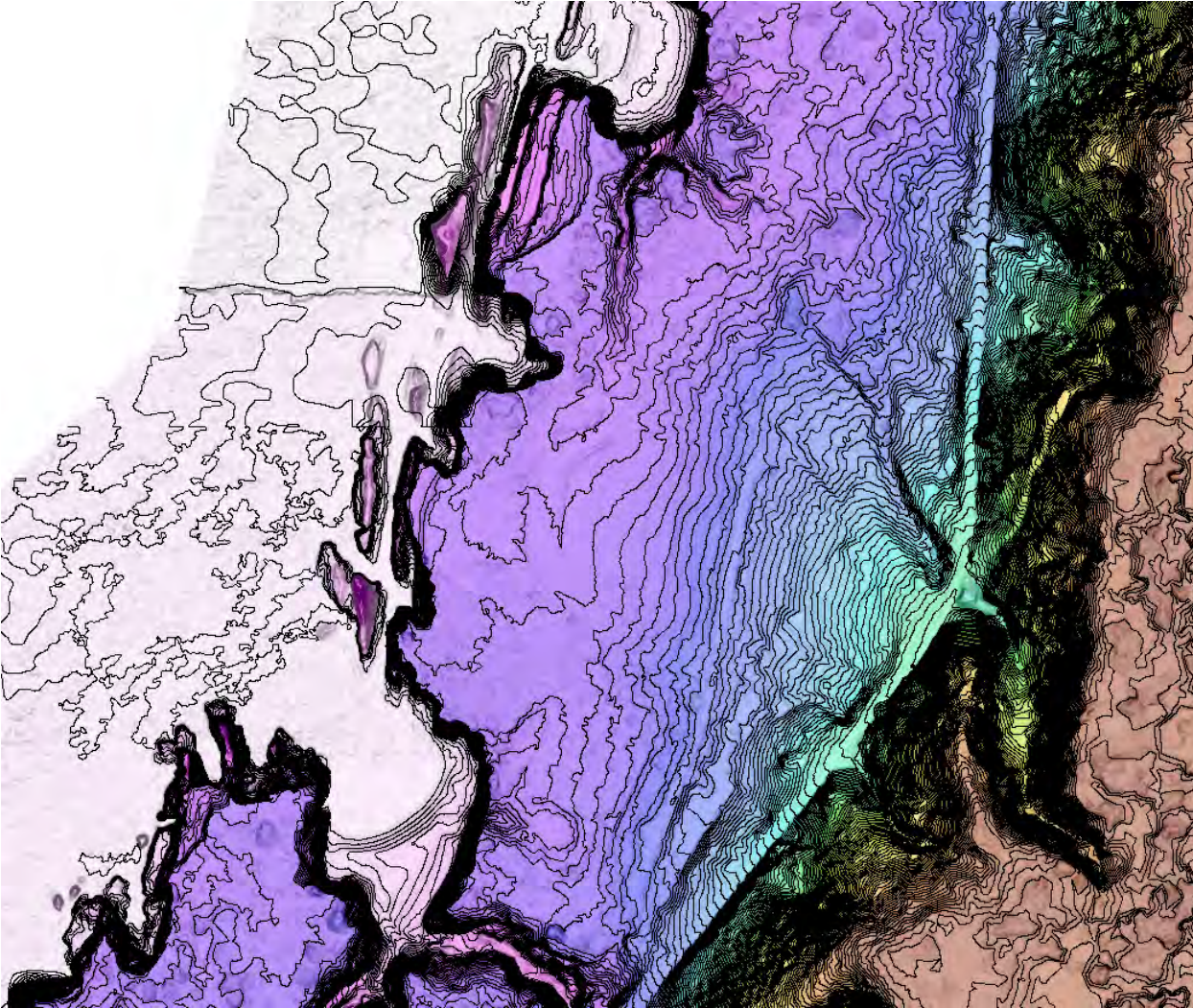


Figure 2-6. 2 ft lidar contours on color elevation gradient and slopeshade at Shore Acres State Park.

Stop 3: Seven Devils Road

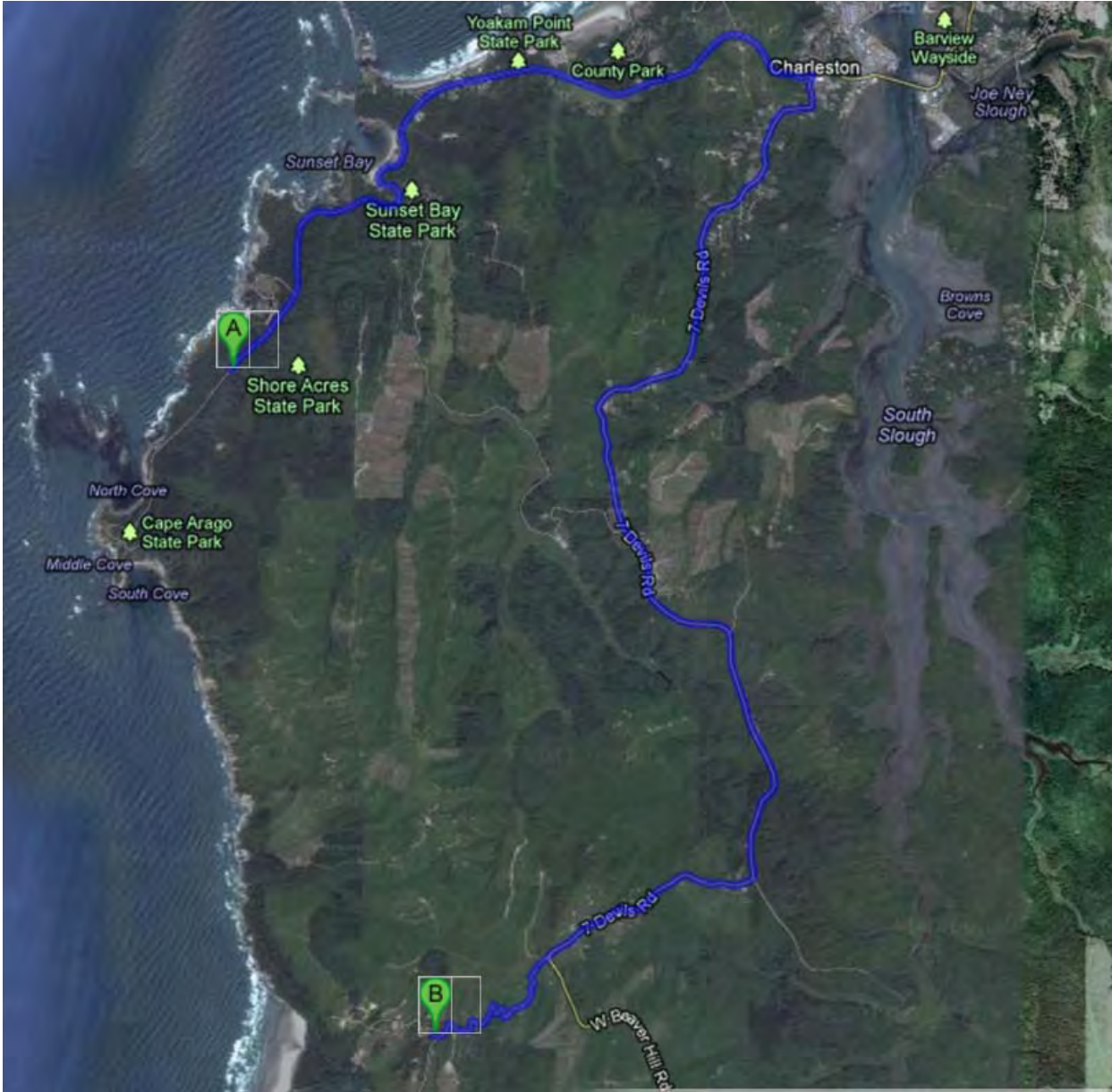


Figure 3-1. Navigation

From Shore Acres to stop 3 is about a half hour drive. We retrace our steps to Charleston then climb quickly up through the marine terrace sequence to get on top of a series of ridges that separate South Slough from the Pacific. These ridges (Figure 3-2) are all capped with Metcalf terrace, which appears as bleached or iron-stained weakly cemented sand. The ridges are all strike ridges held up by the same steeply E-dipping marine strata we saw at Bastendorf beach, with valleys occupying the mudstone intervals. South Slough was long believed to occupy the axis of a large N-trending syncline, but more recent geologic mapping, coupled with gas-exploration seismic shows that in fact there is a thrust fault up the Slough, and our route along Seven Devils road is actually on the anticline formed on the upper plate of the thrust sheet.

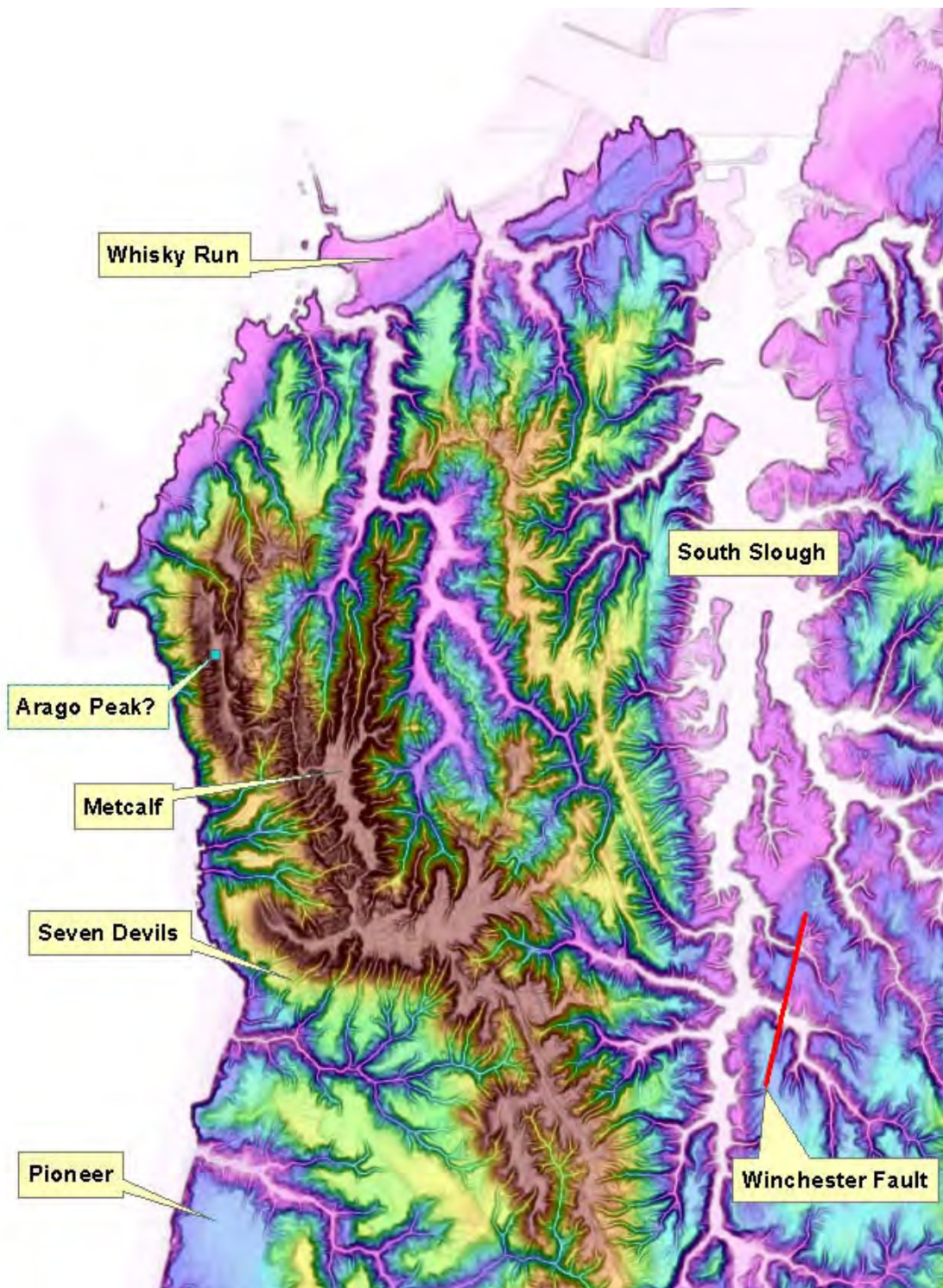


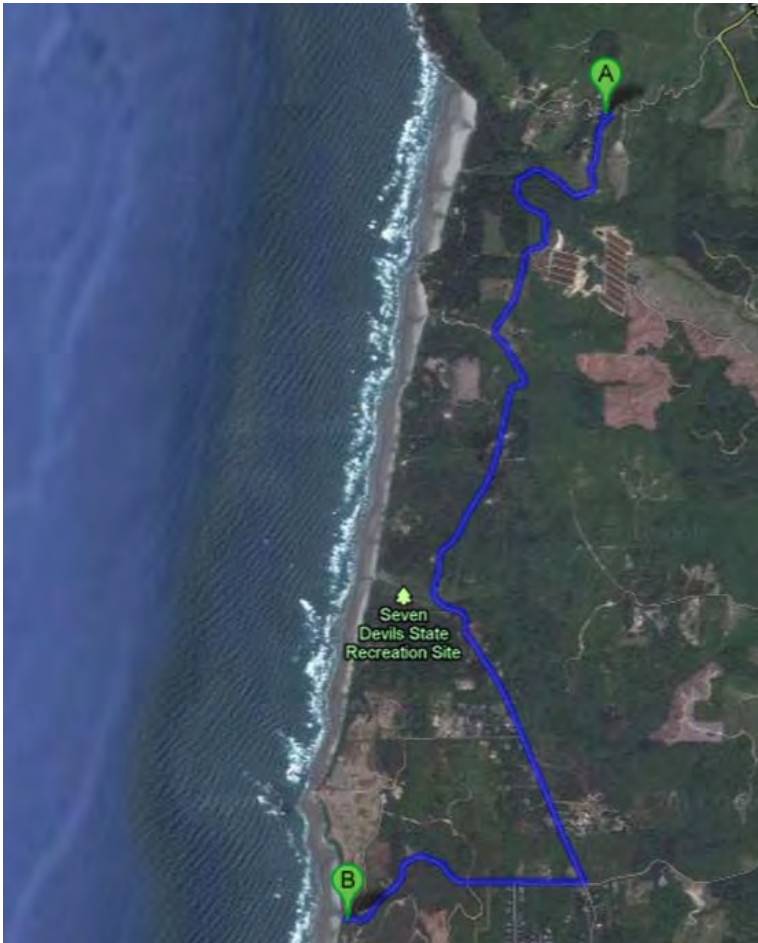
Figure 3-2. Topography along Seven Devils Road.

We turn off the pavement and descend the steep and winding section of Seven Devils road, drive carefully. Everyone but the driver can gawk at the excellent road cut exposures of lower Coaledo Formation sandstone. You may also be able to see the Metcalf wave-cut platform just as we start down; the Metcalf cover sediments here are quite thin.

We will descend to the Seven Devils Terrace and drive across it, stopping just where we start to descend again to look at good exposures of the Seven Devils wave cut platform. Here the platform is cut in lower Coaledo, which is a nearshore

sandstone, and the marine terraces are nearshore sands as well. Both are quite leached or stained with iron and weathered, and it can be very difficult to tell the Eocene from the Pleistocene.

Stop 4: Whiskey Run



Stop 4 is a 15 minute drive from stop 3. En route we will pass the Seven Devils wayside where there are restrooms if needed. We will proceed to the Whiskey Run beach parking lot. About 900 meters after we turn west on Whiskey Run road, we will descend across a scarp about 20 meters high. This has been mapped in the past as the backedge to the Whiskey Run terrace, making the upper surface the Pioneer terrace. We will focus on the scarp at this stop, but lack of good parking and sufficient shoulder (and the lure of the sunny beach!) means that we will discuss it down at the parking lot. McNally and Kelsey (1990) mapped this scarp as the Whiskey Run backedge, and the high surface to the east as the Pioneer Anticline, an area of warped Pioneer terrace surface, and the Pioneer anticline is actually a seismic source in the USGS NSHM model, with a slip rate of 0.2 to 1mm/year. This scarp is unusually straight and sharp for a Whiskey Run backedge, but the orientation and scale are certainly consistent. I propose new high resolution nearshore bathymetry provides evidence that this feature is in fact a fault scarp. Figure 4-3 shows

recently acquired offshore data along with the lidar, and there is a strong linear feature in the submarine bedrock that is exactly on strike with the scarp. The lidar also shows evidence that the scarp divides and steps (Figure 4-4) right, developing a small graben just before it goes offshore, which is not behavior consistent with a sea cliff.

If we take a wider look, the lidar reveals several other even more convincing fault scarps (Figure 4-5) in the marine terrace surface, two of which cannot be backedges because they face landward. Although many of these scarps are quite large, they are cutting a surface that is 80-105 ka in age, so their slip rates are modest. Given the proximity to the subduction zone, there is a question as to whether these faults have an independent seismogenic movement, or simple slip sporadically with subduction events.

This is not the first evidence for active faulting in the area. Back in the early 1990's, Mark Hemphill-Haley and I trenched an 8 m high scarp in the Seven Devils or Metcalf terrace on the Winchester Fault, located at the south end of South Slough (Figure 3-2). We found a beautiful west dipping fault (Figure 4-6) that thrusts Coaledo formation over the marine terrace cover sediments and soils. The wave cut platform is drag-folded on the upper plate, standing vertical, then overturning into the fault plane, dragging beach lag boulders on the platform with it. Three separate colluvial wedges suggest at least two earthquakes, but radiocarbon samples from all but the youngest unfaulted colluvium were carbon dead.

McInelly and Kelsey defined the Pioneer Anticline using the water wells that they could locate in the later 1980's to define the elevation of the wave cut platform. Development over the last few years has greatly increased the number of wells in the area, and offers an opportunity to revisit this problem with better data

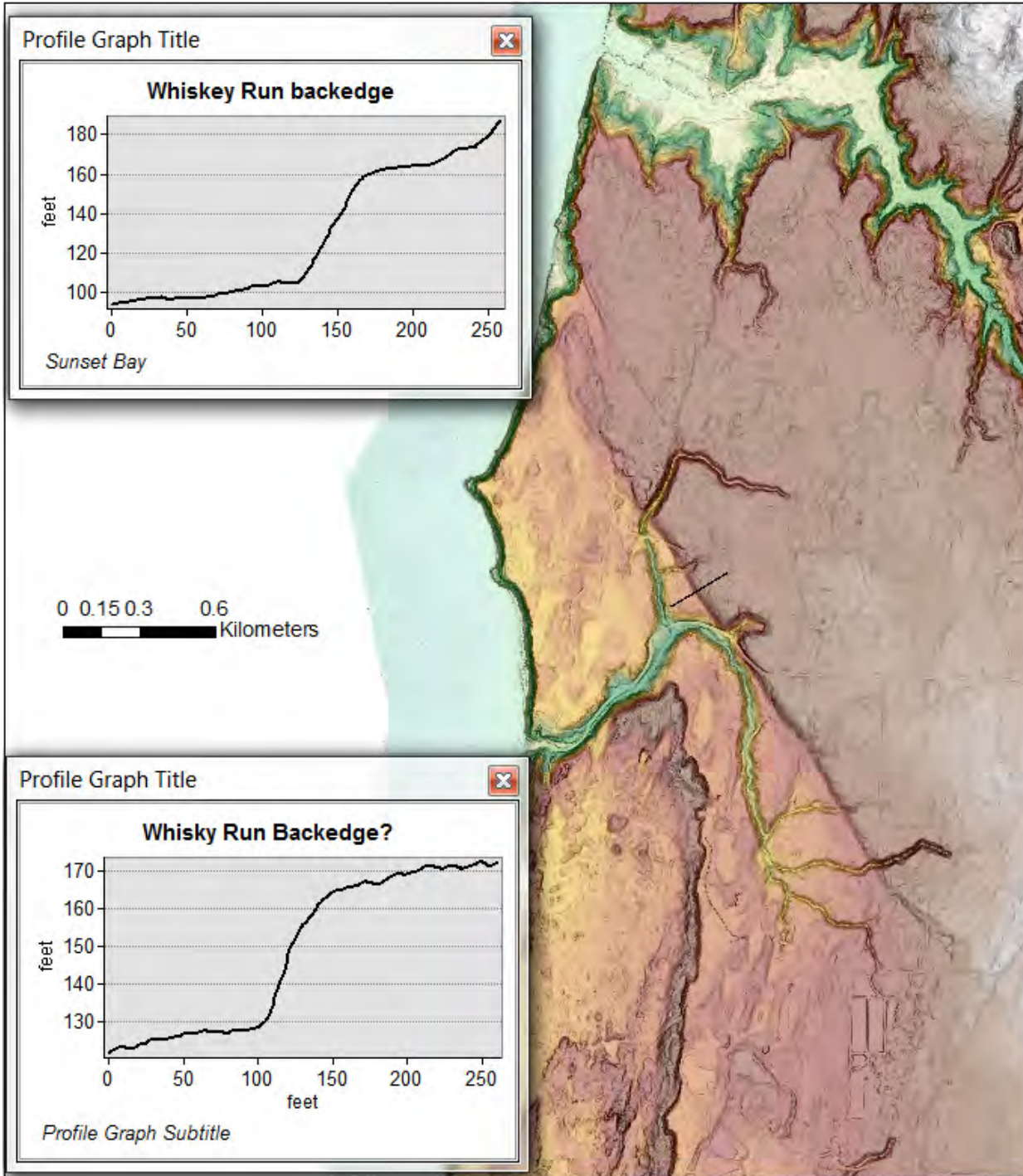


Figure 4-2. Whiskey Run backedge/fault?

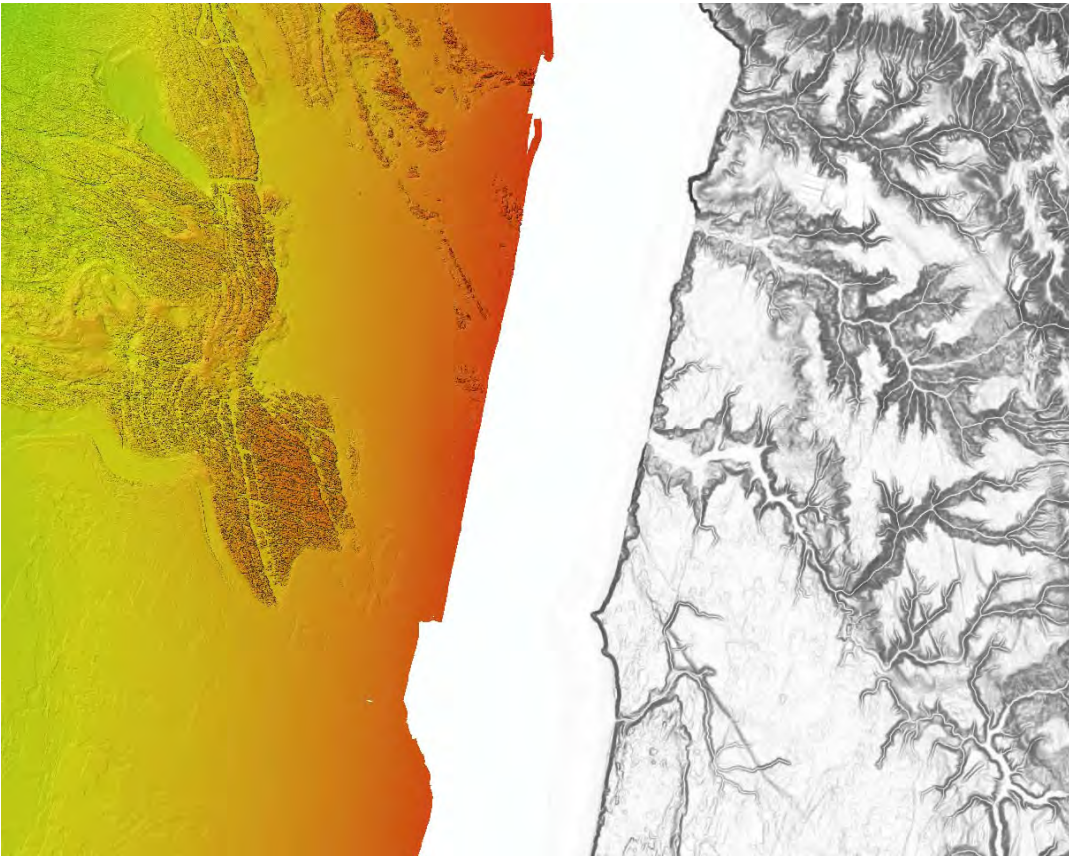


Figure 4-3. Lidar and high-res bathymetry

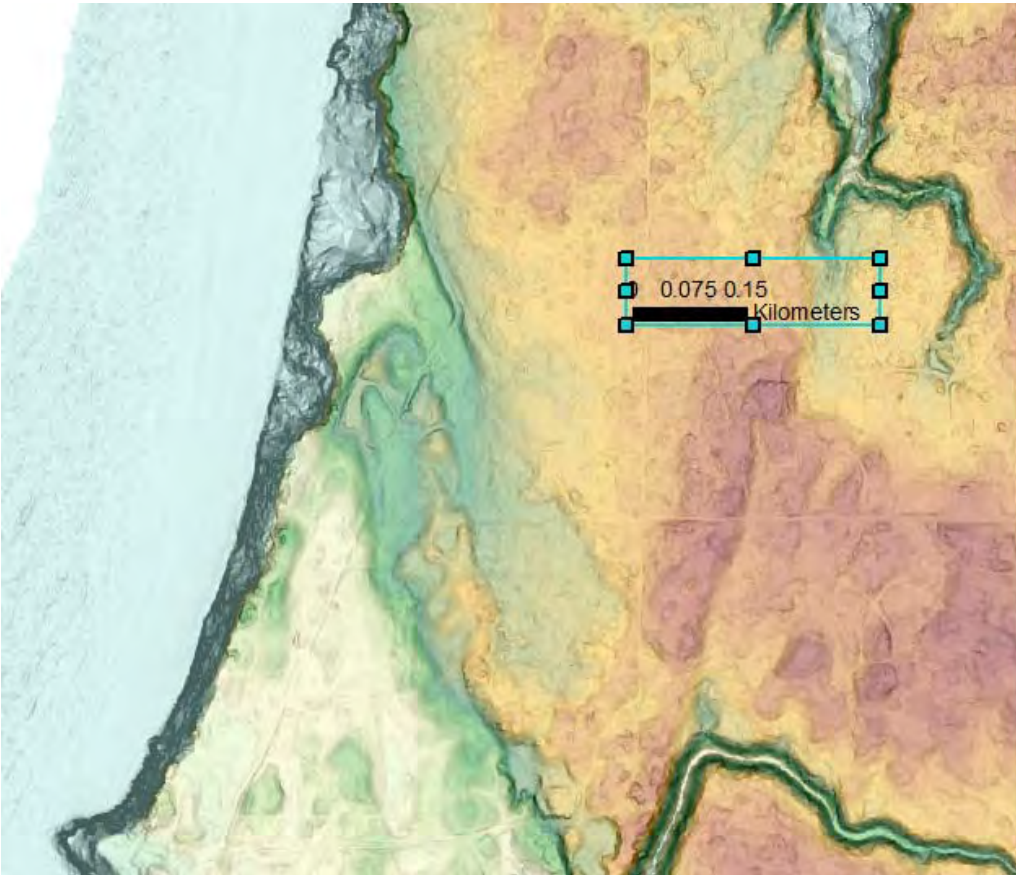


Figure 4-4. Detail of Whiskey Run backedge/scarp

Finally, a note about Whiskey Run. The name originated during the local gold rush in the late 1800's, when miners worked some placers in the marine terrace. Today, these same black sand placer deposits are being mined from the Seven Devils terrace just west of Whiskey Run by Oregon Resources Corporation. The primary product of the mine is refractory chromite for casting, but the black sands also contain ilmenite, garnet and minor gold and platinum. These minerals are absent in the local marine sedimentary rock, and are derived from the Jurassic accreted terrains to the south and southeast of here.

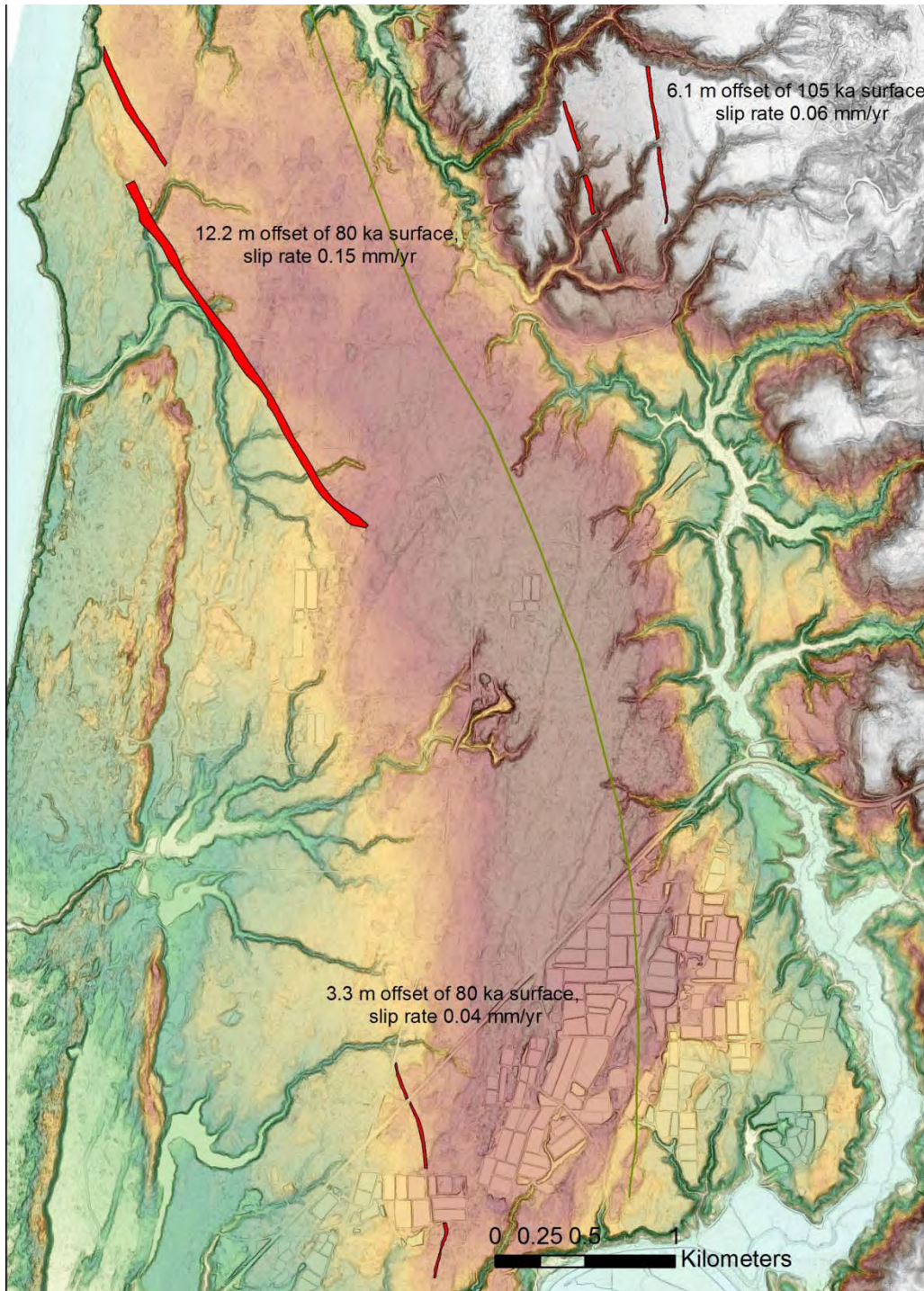
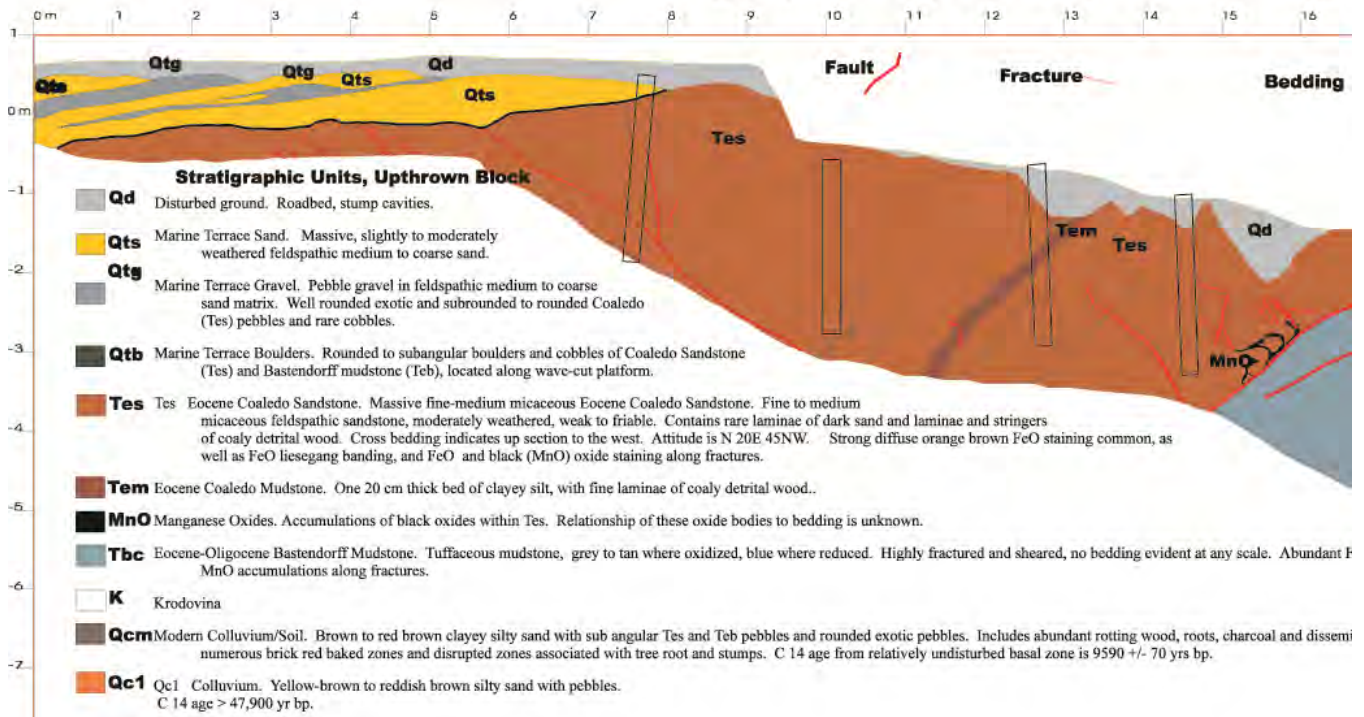


Figure 4-5. Scarps on the Pioneer Anticline

Winchester Fault Cox Can

N 85 W

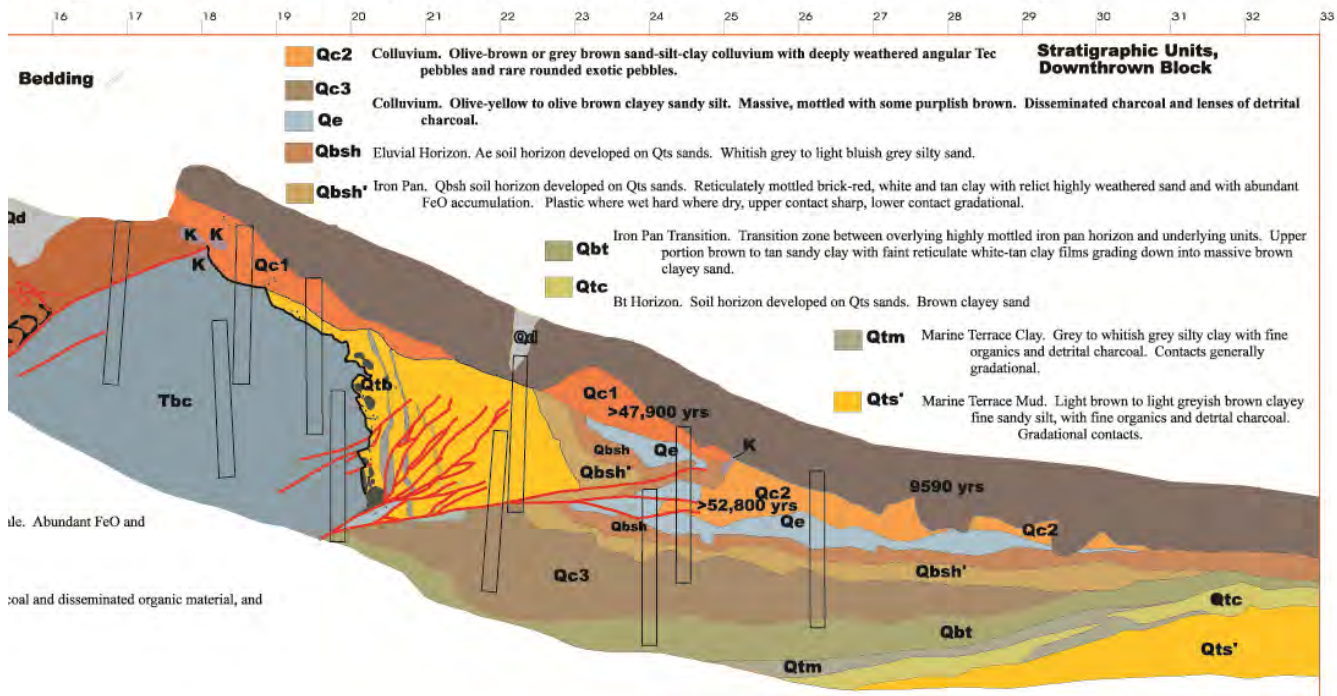
Logged September 1993 by Ian Madin (Oregon Department of Geology and



Canyon Scarp, Trench A, Coos County, Oregon

S 85

(Geology and Mineral Industries) Mark Hemphill-Haley (University of Oregon) and Tim Roberts (Oregon State University)



Figure

4-6. Winchester Fault trench log.

Stop 5: Bullard's Beach

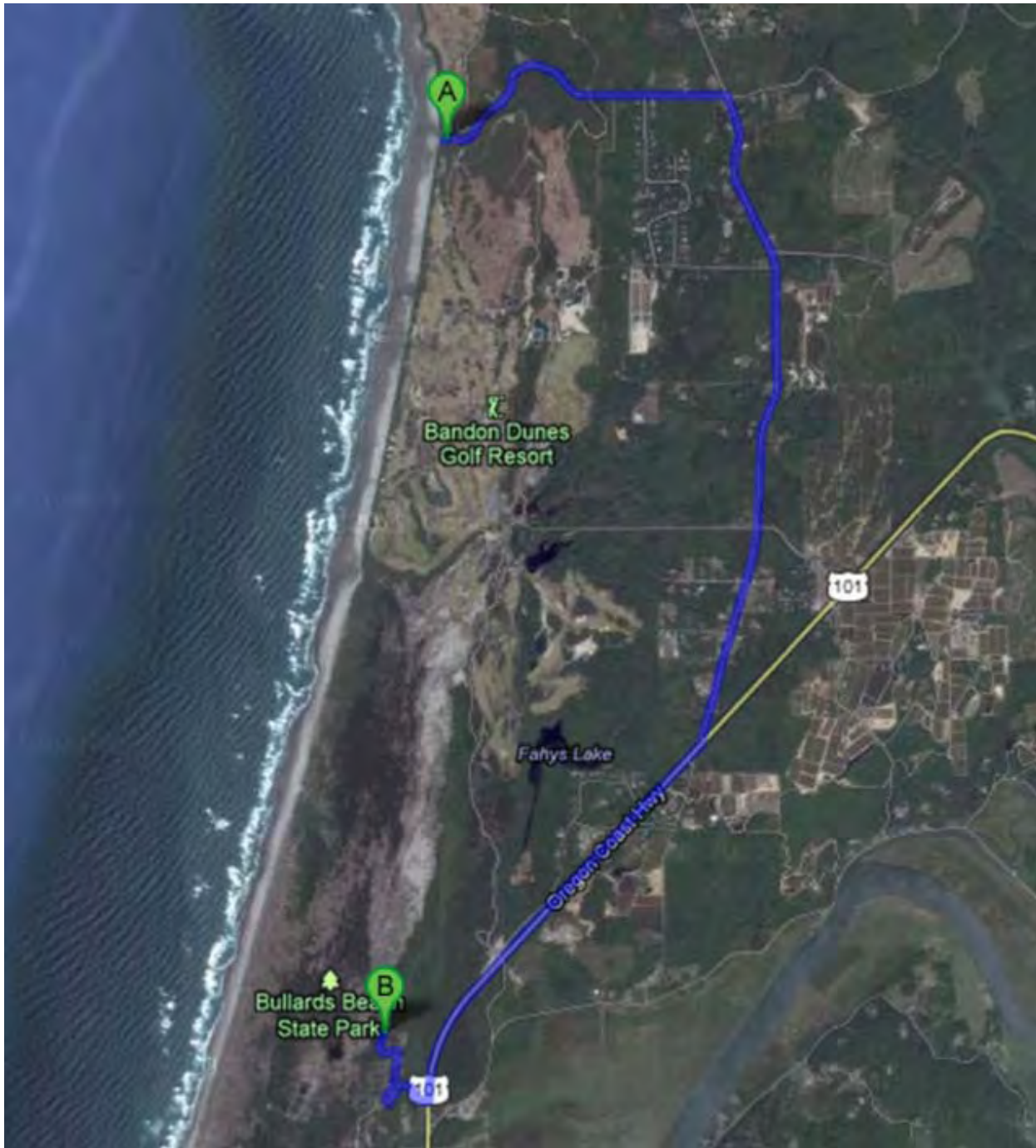


Figure 5-1. Navigation

From stop 4 we retrace our steps to Seven Devils road then turn south to meet Hwy 101, reaching Bullard's Beach state park in about 15 minutes, where we will meet at the picnic shelters in the day use area for lunch. A few hundred meters before we reach the intersection of Seven Devils road and 101, we will cross the southernmost scarp on Figure 4-5, see if you can spot it!

At Bullard's beach we are sandwiched between the Coquille River and the Pacific both of which have the potential to cause flooding in and around Bandon. FEMA issues Flood Insurance Rate Maps, which define AE zones, areas in which flood insurance is required. These maps are developed by calculating the water surface elevation expected from the 100 year flood. These hydraulic calculations are performed at numerous transects using surveyed floodplain and channel geometry, and are precise to a fraction of a foot (accuracy is another matter, but most of the uncertainty stems from the aleatory uncertainty of flood flows). To make the flood rate maps, the flood water surface defined by the transects is intersected with the topography, and a line is drawn along that intersection. However for most of Coos County, the best available topographic maps have 40 ft contours, meaning they have ~ 20 feet of vertical uncertainty, making the flood zone boundaries largely meaningless. In 2008, DOGAMI collected high resolution lidar with vertical accuracy of 5-10cm from most of Coos County, and convinced FEMA to pay for a pilot project to redelineate the flood zones. In essence, we followed the same procedure as before, but this time using topographic data with the same precision as the modeled transects. The resulting new flood maps caused about as many negative as positive changes, but have the advantage that the results are now reliable.

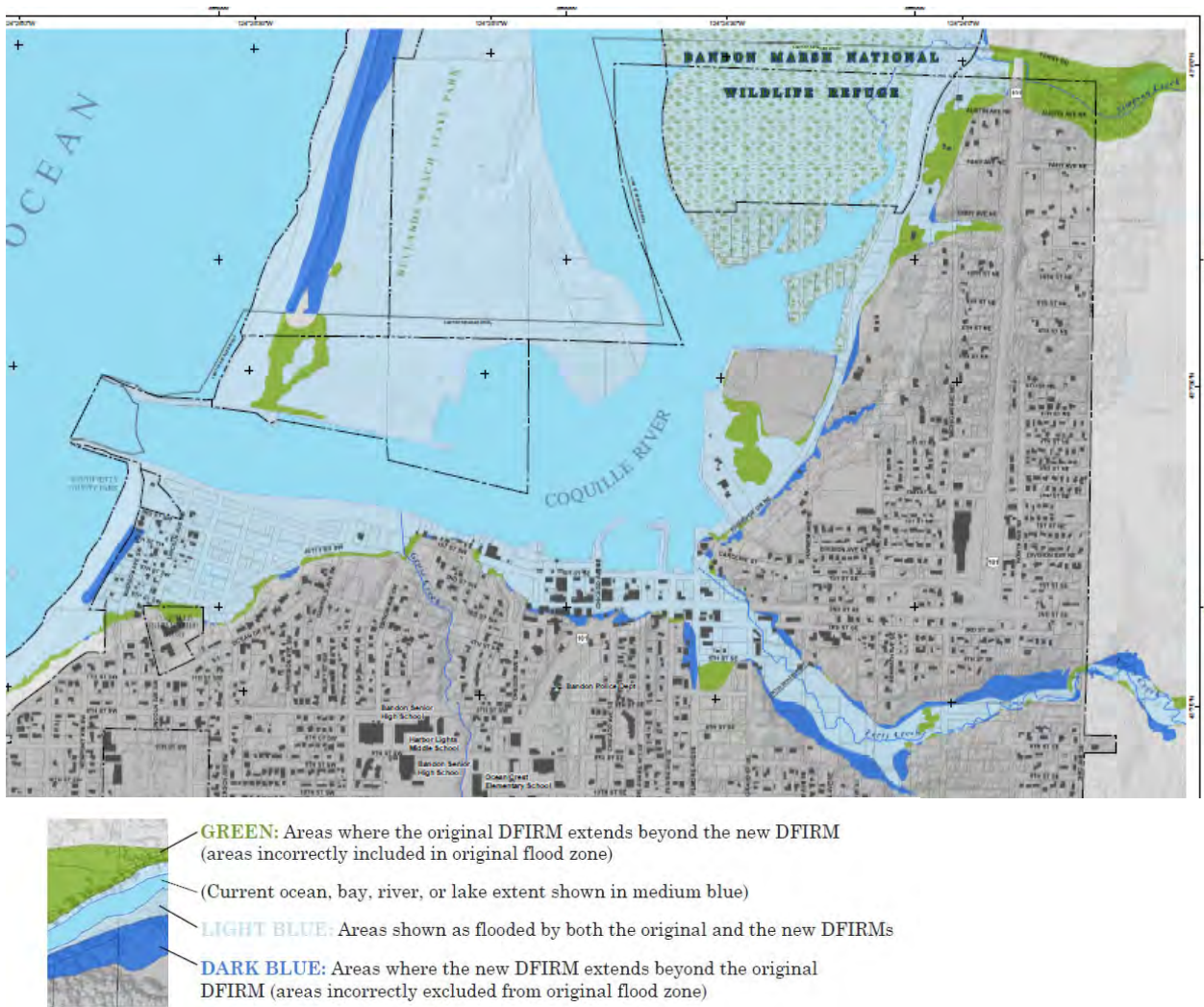


Figure 5-2. Redlined DFIRM change map for Bandon.

An additional application of lidar for flood hazard mapping is risk and exposure mapping. Building footprints can be cheaply extracted from high resolution lidar, allowing us to build a very detailed and accurate model of the built environment. By overlaying detailed hazard information on the building model, it becomes possible to determine which buildings are exposed to the hazard, and in the case of flood maps, the degree of hazard, in this case depth of flooding.

Figure 5-3 shows the flood risk map for Bandon, buildings exposed to the flood are color coded by depth of flooding, with yellow representing 0-3 feet of flooding, orange 3-6 feet, and red greater than 6 feet. Flooding in the 0-3 foot range generally only requires cleanup, whereas in the 3-6 foot range, extensive repairs are required, and at depths greater than 6 feet, most buildings are a total loss. It is also sobering to note that the 100-year trend in precipitation in the region has been an increase from an average of about 47 inches per year to almost 60, suggesting the flooding will get worse in the future. The two extreme precipitation outliers are the 1996 and 1998 El Nino years.

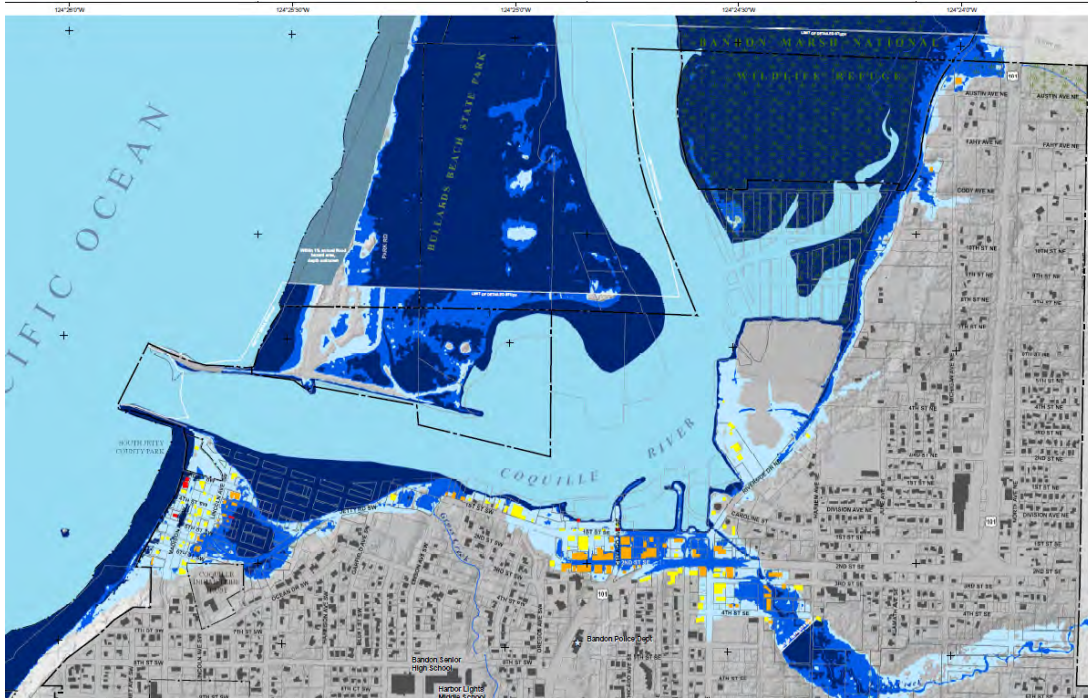


Figure 5-3. Bandon flood risk map

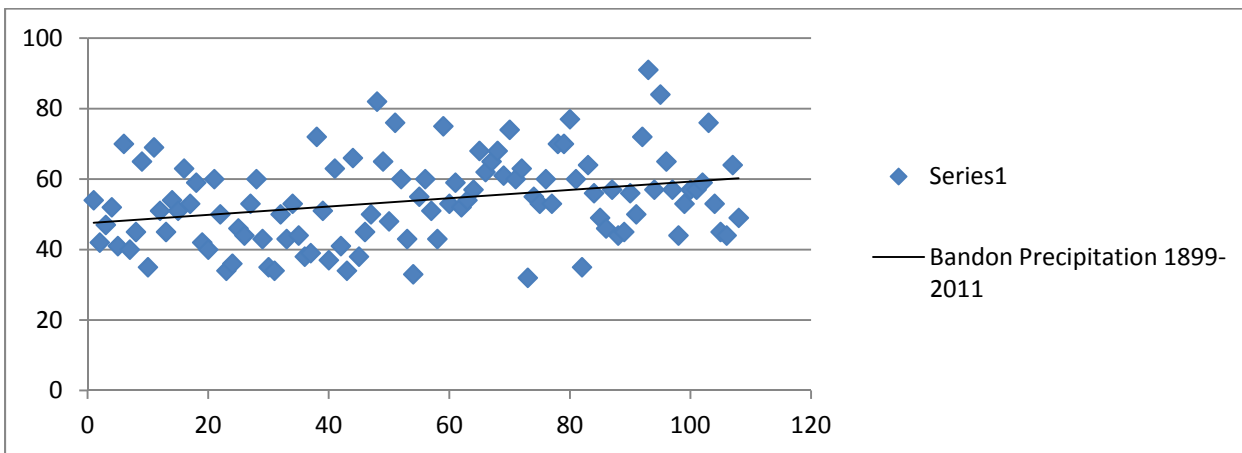


Figure 5-4. Bandon precipitation trend

The sharp eyed among you will notice that the crest of the dune along the spit in Bullard’s Beach park has been added to the flood zone in Figure 5-2, with flooding to an elevation of 28 feet, well above the maximum flood in Bandon of about 16 ft. This is the result of new mapping of the coastal V and VE zones, which define coastal areas subject to wave flooding at the same 100 year recurrence. In this case however, it was not a simple matter of putting existing flood

elevations on the new lidar topography, and instead Jonathan Allan at DOGAMI developed a new methodology for determining the VE zones starting with the fundamentals of the Oregon wave climate. We touched on the how energetic and seasonal Oregon's waves are back at stop 1. For mapping the VE zones, we need to know the likelihood of particular levels of flooding, therefore we need to look at the combined effect of waves and ocean water levels (tides, El Nino's, storm surges) in order to forecast future probabilities just as we use historical flood records to calculate future flood probabilities.

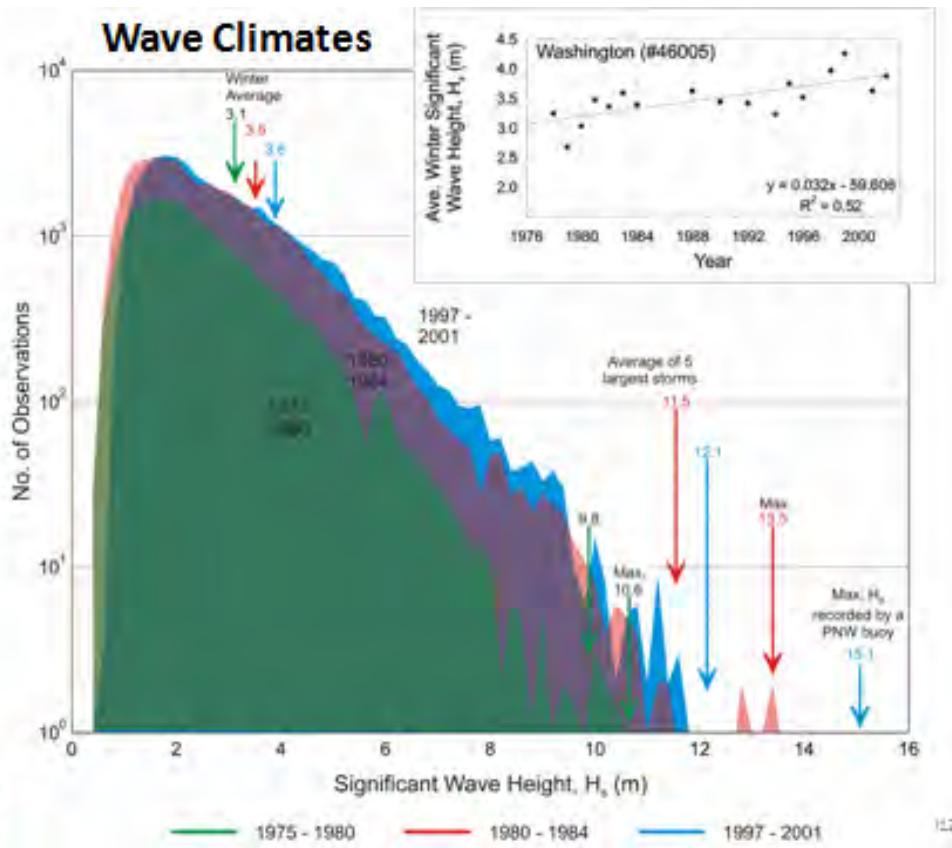


Figure 5-5. Trends in PNW wave climate from 1975 to 2001.

Good wave climate data from several offshore buoys are available for almost 40 years, and the plot in Figure 5-5 shows an interesting and alarming trend. Just like the precipitation at Bandon, the average significant wave height as well as the maximum wave height have been steadily increasing, to the point where waves that would have been considered hundred-year events 30 years ago, are now 10 year events. This has tremendous implications for flooding during big storms, as well as coastal erosion, because bigger waves carry much more energy (energy content increases as the square of significant wave height) and cause much more of a storm surge, resulting in much higher wave flooding elevations. This is a problem not only because of inundation, but because erosion of the primary frontal dunes that back many Oregon beaches and protect or support many homes and other buildings is directly a function of the extreme water level that is reached during a storm event. Figure 5-6 shows the model that is used to calculate erosion potential on dunes, and clearly higher water levels resulting from more energetic waves will lead to accelerated erosion. Now remember the European beach grass from stop 1? The stabilization of these foredunes over the past 40 years has provided developers with a false sense of security, leading to extensive building programs out along the spits and on the frontal foredunes themselves. Coincidentally, the increase in wave energy over that same period is now causing the ocean to erode the higher and more stable dunes increasing communities' risk from both erosion and flooding. In response to these hazards, the shorelines in many of these communities are having to be "fixed" with coastal

engineering structures in order to safe-guard the properties (e.g. Alsea and Siletz Spit (Lincoln County), and Neskowin and Rockaway in Tillamook County) (Figure 5-7).

Finally, what about global warming and sea level rise? Barring ice-sheet collapse, most projections for global-warming-induced sea level rise are in the 2-4 mm/yr range, with some projections suggesting that sea level will rise by up to 1 m by 2100. In a typical Oregon winter we see a sea level rise of over 20 cm, and in years with strong El Nino's, it can be as much as 50-60 cm. This annual sea level rise results from the fact that the water off the coast of Oregon is actually warmer in winter than in summer, as the summer wind patterns tend to cause upwelling of much colder deep water. Simple thermal expansion of that warm (hard to think of the ocean off Oregon as warm in the winter, it is all relative) water causes the increase in sea level. Between this and the dramatically strengthening wave climate, we are getting a glimpse of the future, and it does not bode well for the future of beachfront homes in Oregon. In fact, the only thing working in our favor these days is the tectonic uplift associated with the steady loading of the Cascadia Subduction zone that actually makes the south coast emergent. The problem of course is that at some point we have to give all that back, but that will be the subject of the next stop.

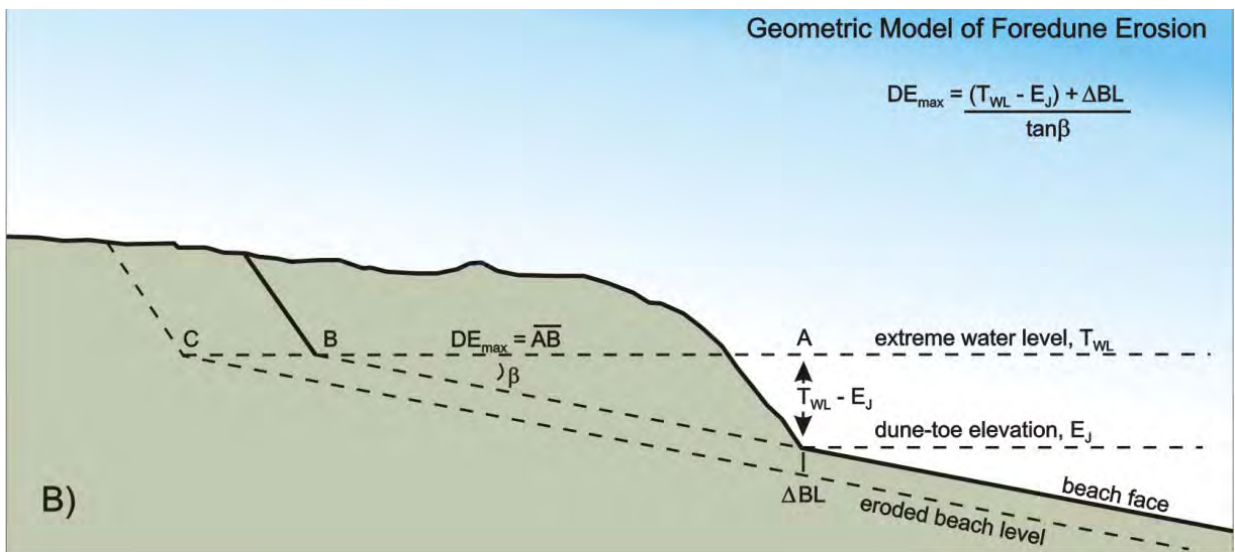


Figure 5-6. Erosion model for dune-backed beaches. The assumption is that storm waves always have sufficient energy to erode sand, so that if a given extreme water level is maintained, erosion will proceed until the dune-toe elevation has migrated up the beach face to the elevation of the extreme water level.

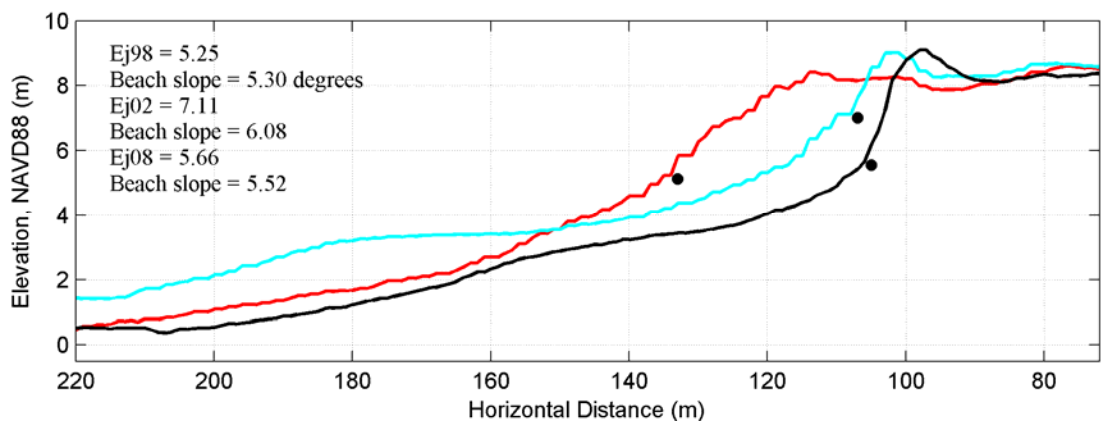


Figure 5-7. Recent erosion at Coos Spit, just north of our stop 1. Red is profile from 1998 lidar, blue from 2002, and black from 2008. The beach dune junction has retreated about 30 meters in 10 years

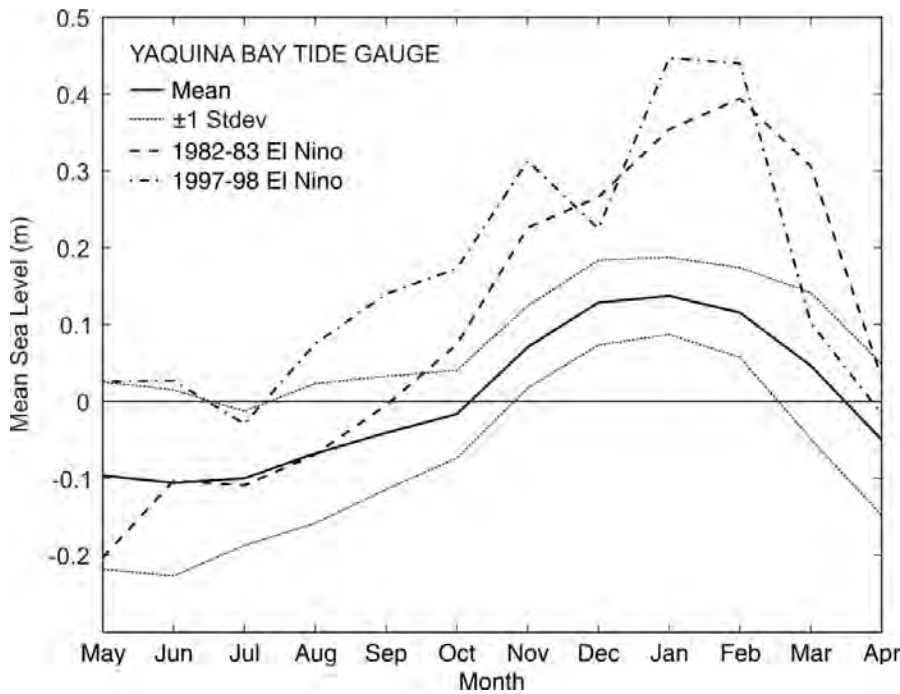


Figure 5-8. Annual sea level changes at Yaquina Bay.

We are all broadly familiar with the fact that the Cascadia Subduction zone is known to have generated numerous megathrust earthquakes as large as M 9 over the last 10,000 years. The initial paleoseismic evidence for these events came from coastal marshes in Washington and Oregon, where forest or freshwater marsh deposits were found to have been abruptly converted to tide flats by coseismic subsidence, in some cases producing spectacular buried forest. The marsh adjacent to our lunch stop was studied extensively by Rob Witter, Harvey Kelsey and Eileen Hemphill-Haley.

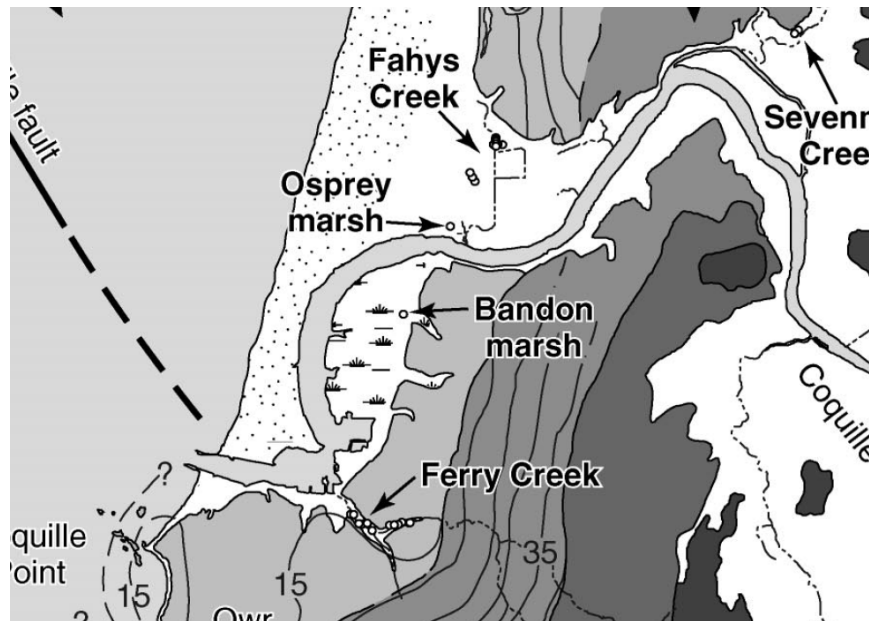


Figure 5-9. Bandon paleoseismic core sites. Witter et al, GSA Bulletin 2003.

The cores here record 6 burial coseismic burial events in the last 4500 years (Figure 5-10), and the record from all the marshes cored in the area includes 12 events spanning 6500 years.

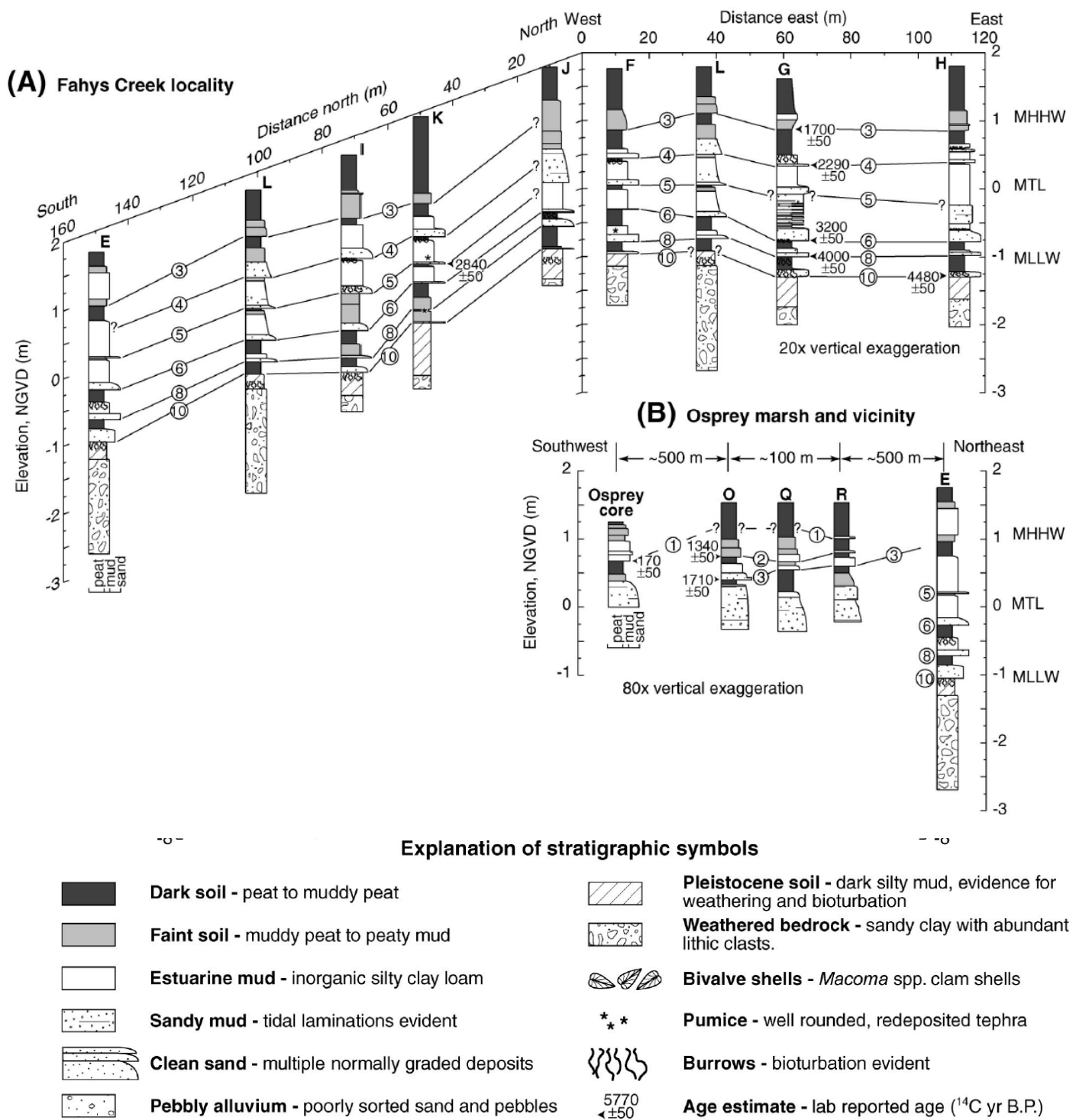


Figure 5-10. Correlation of cores at Bullard's Beach park, Witter et al, GSA Bulletin 2003

Stop 6: Bradley Lake

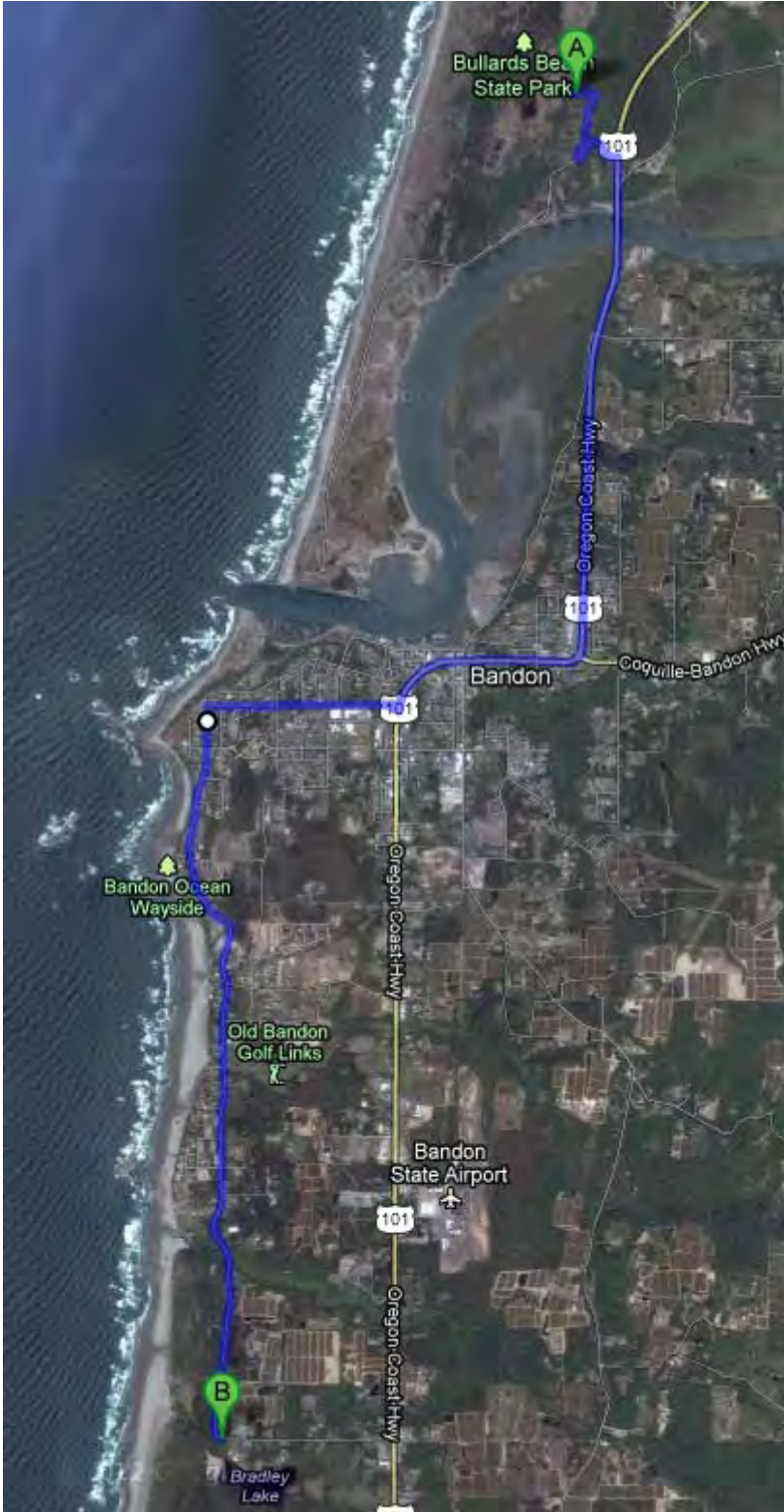


Figure 6-1. Navigation.

From Bullard’s Beach we proceed south on 101 to just south of Downtown Bandon, then turn west on 8th street to the Beach Loop Road where we turn left. As we proceed south along the bluff, you will notice lots of offshore rocks, but unlike at Shore Acres, these define no obvious structure. We have left behind the Eocene sedimentary rocks, and the bedrock here is Jurassic Otter Point formation, a mélange with abundant knockers which form the many sea stacks. The most famous of these rocks was a huge blueschist knocker in downtown Bandon, sacred to the native peoples, that was completely quarried out to build the Bandon jetty. It is some of the most beautiful rip rap you can imagine, but at a huge cultural cost. We continue south to the Lake Bradley Christian Retreat. We have permission to park on Retreat property, and then hike to the dune that dams Bradley Lake for our discussion. There will be a retreat in session so please be quiet and respectful as we travel to the dune.

We discussed the record of past subduction zone earthquakes preserved in buried marsh deposits at the previous stop, and most are probably aware that Chris Goldfinger at OSU has established (and in the last month published) a detailed 10,000 year chronology of megathrust events that includes 19 full margin ruptures and an additional . Chris’ excellent record is based on deep sea cores of turbidites triggered by the strong shaking from past events. It was necessary to look in the deep ocean for a long record for the simple fact that Holocene sea level rise has been

moving the marshes used for the terrestrial record inland, so that older events are now under water or eroded away. Bradley Lake however provides a third way. The lake has formed where a dune has dammed a small stream, and the dune crest is currently about 36 feet above sea level and the outlet stream about 22 feet, both high enough that even

the largest storm surges do not enter the lake (though we will see if that changes in the next few decades after what we learned at stop 5, where the modeled 100 year wave flooding reached elevations as high as 28 feet!). Harvey Kelsey, Alan Nelson, Mark Hemphill-Haley and Rob Witter realized that the elevation of Bradley Lake was at the ideal elevation to record large tsunamis generated by local Cascadia earthquakes while filtering out storm surges and distant tsunamis. They collected sediment cores from the lake bottom, that ultimately revealed a record of tsunamis and local strong shaking that extends back 7500 years (Figure 6-3). The normal sediment deposited in the lake bottom is laminated mud, but from numerous cores it is apparent that the mud is interrupted by 13 landward-thinning sheets of sand, typically containing marine diatoms, that represent the deposit left by tsunami incursion into the lake during past Cascadia megathrust earthquakes. An addition 4 disturbances that only show interruption of the laminated mud by organic mud and detritus are interpreted as evidence for shaking without tsunami inundation, perhaps some of the segment C or D ruptures shown in Figure 6-2, that did not produce a tsunami large enough to inundate the lake.

This record, which directly records the tsunami generated by a megathrust, can be compared with the chronologies developed from marsh cores that record elastic coseismic subsidence and the turbidite record that records strong shaking. Figure 6-4 shows such a comparison, in which 21 events have been correlated between all records, and another 8 can only be correlated between a few. Due to the uncertainty involved in dating an instantaneous event like an earthquake with radiocarbon, and the difficulty of comparing terrestrial and marine radiocarbon ages, it is not possible to conclusively correlate any single event among the various sites, but the overall pattern remains quite convincing. This evidence, coupled with the evidence for the segmentation shown in Figure 6-2, and evidence developed in Professional Paper 1661-F that relates turbidite mass to megathrust size allows us to create a chronology that also includes information about the relative size of past events.

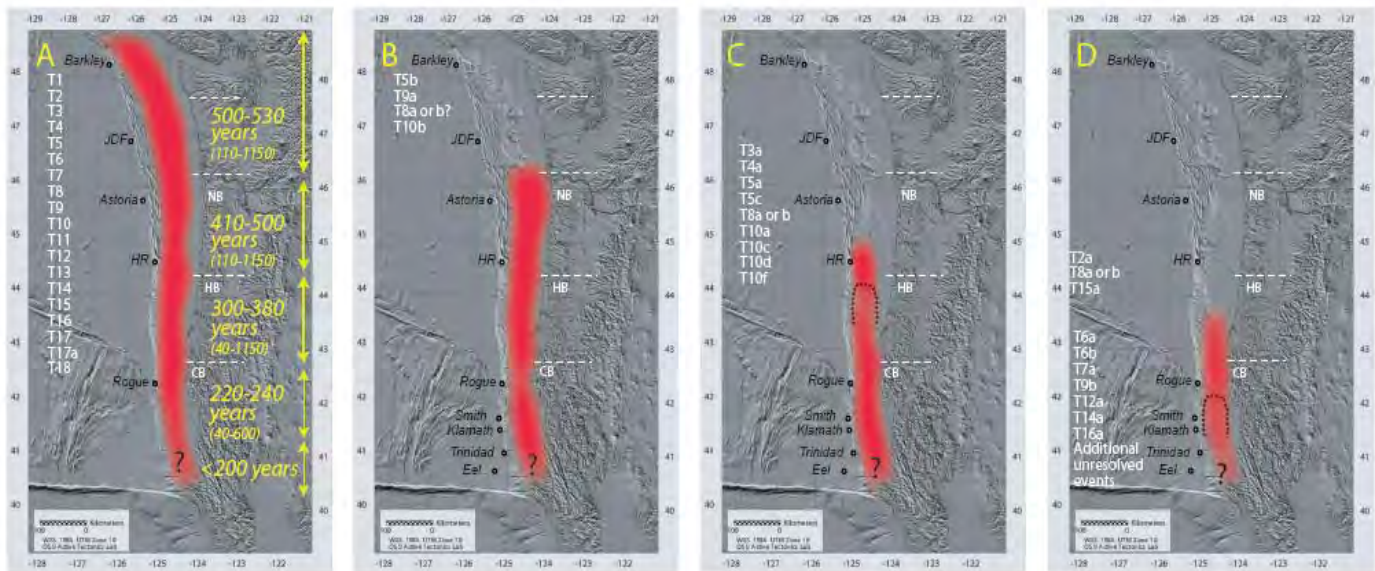


Figure 6-2. Cascadia megathrust rupture modes and event tallies from USGS Professional Paper 1661-F

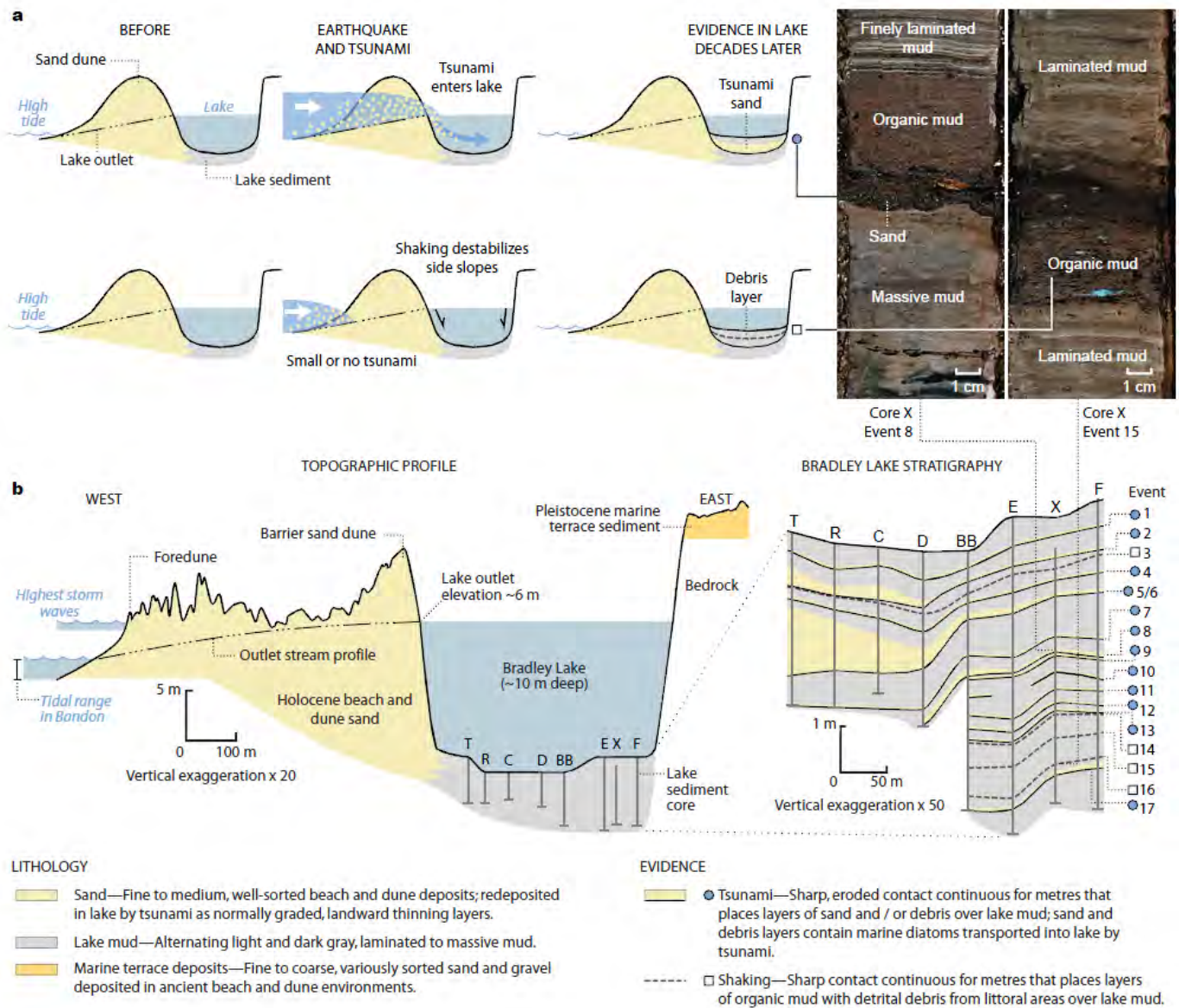


Figure 6-3. Figure from in preparation paper by Rob Witter, Yinglong J Zhang, Kelin Wang, Chris Goldfinger, George R Priest and Jonathan C Allan, please do not reproduce or cite.

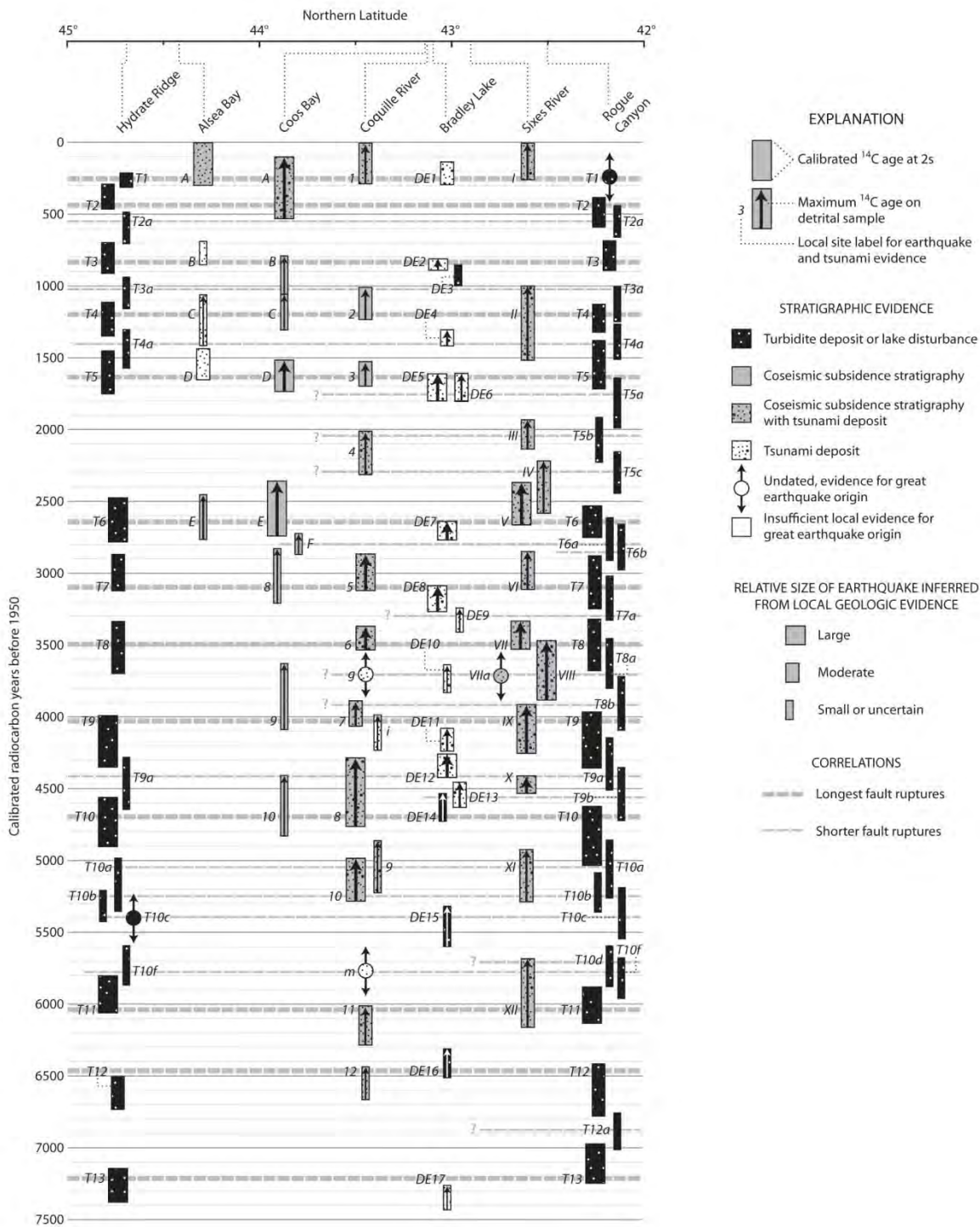


Figure 6-4. Figure from in preparation paper by Rob Witter, Yinglong J Zhang, Kelin Wang, Chris Goldfinger, George R Priest and Jonathan C Allan, please do not reproduce or cite. Correlation of Cascadia megathrust paleoseismic records.

For the last 4 years, DOGAMI has been preparing new tsunami inundation maps for the Oregon coast in an effort led by George Priest and Rob Witter. Since the ghastly images of tsunami inundation in Tohoku, it has become very clear that if you are in the inundation zone, you are screwed, whether you are a person or a building, so defining the likely inundation zone for our next Cascadia megathrust is essential. Tsunami modeling has four steps. First you must determine the likely shape of the coseismic sea floor deformation that displaces the ocean. Next you must propagate the tsunami through deep water, then calculate the dramatic changes that occur as the wave enters shallow water, and

finally model how the wave moves across and interacts with the terrestrial landscape. The last three steps boil down to the physics of moving waves in water, which although fiendishly difficult to calculate, is well-understood. The calculations are done by Joseph Zhang at OHSU, using a model called SELFE. The main challenges here are getting accurate bathymetric and topographic data. DOGAMI has solved this problem by building custom bathy-topo computational grids using the best available bathymetric data and lidar for the terrestrial portion. The resulting grid has 1.4 million nodes and 2.8 million triangles and extends clear to Alaska. The resolution is crude in deep water, becoming progressively more refined as it approaches the shore, and on land can be as fine as 1m. By far the most difficult part of the problem is defining the seafloor deformation. There is a large amount of uncertainty as to the amount of slip that will occur in the next event, and in how that slip will translate into deformation at the surface. Figure 6-5 shows an example of the combined effects of slip and deformation mode. This makes a huge difference, for a given deformation shape, tsunami runup scales linearly with slip, and there are large differences between the runup produced by uniformly distributed slip and slip on a shallow splay fault. Needless to say, the number of possible combinations is endless, and there is little basis to predict what the next event will look like. DOGAMI's approach was to run numerous simulations for two test areas, Cannon Beach and Bandon. A wide range of models were tested, based on a careful evaluation of all available geologic and geophysical information that might favor one model over another. Once the sensitivity of the parameters was understood, we selected the deformation mode that produced the largest tsunami for a given slip, in order to provide conservative results. This turns out to be the splay fault model, and there is good evidence in the offshore geology revealed by bathymetric and seismic surveys for the evidence of such a fault. We then selected a of 5 possible earthquake sizes; Small (9.5 m slip), Medium (14.4 m slip), Large (22m slip), Extra large (35m slip) and Extra Extra Large (38m slip). These five events are now being modeled for the entire coast along with a repeat of the 1964 Alaska tsunami, and a model of the largest plausible Alaskan tsunami.

Bradley Lake has played a key role in this effort, because it has recorded many past tsunamis, so the modeled events need to be able to reproduce what is seen here. As a result, DOGAMI undertook a sensitivity analysis of the tsunami model here in order to see what parameters were necessary to get the wave into the lake. The initial results, using the modern topography, required an earthquake with 500 to 600 years of slip deficit to get into the lake for distributed slip models, and 460 years of slip deficit using the splay fault model. This is a problem, because the majority of the recurrence intervals for this section of the margin are shorter, with an average of 240 years, suggesting that past events had an easier time getting into the lake. DOGAMI then tested several different configuration of the coast (Figure 6-6) to see how plausible changes in the topography over the last hundreds or thousands of years might affect the size of tsunami needed to get into the lake. Although these changes shortened the intervals needed to generate large enough waves, even the shortest remain much longer than the average paleoseismic interval, suggesting that using recurrence intervals as proxies for slip is incorrect.

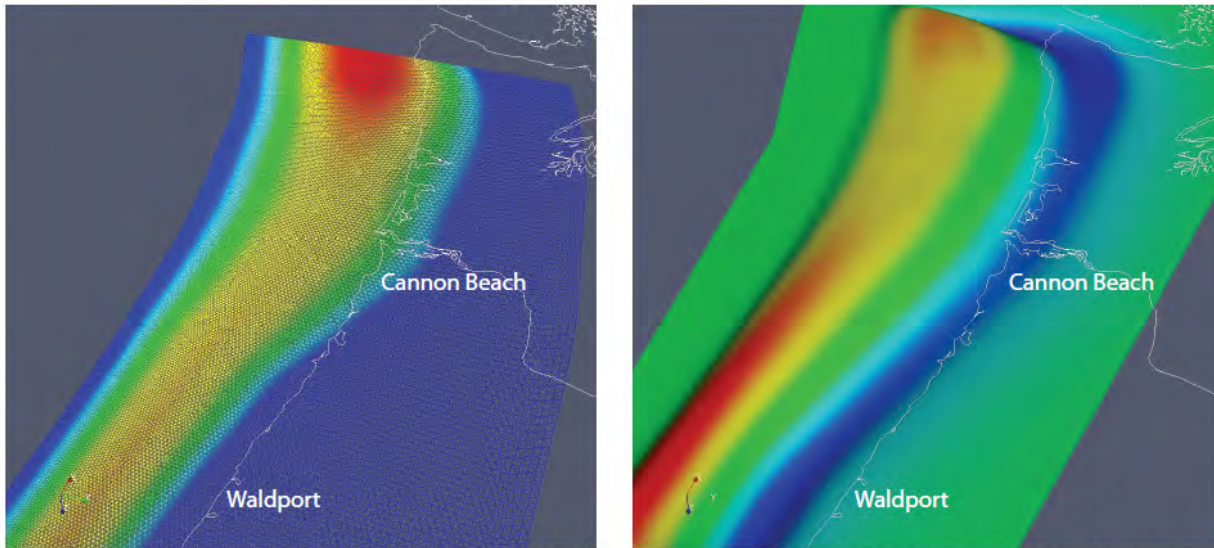


Figure A5. Fault slip distribution (left) and resultant surface vertical deformation (right) for the no-splay-fault model of medium p2a patch with modified symmetric fb76 slip distribution. Red is ~17-18 m slip (left) and ~3 m uplift (right).

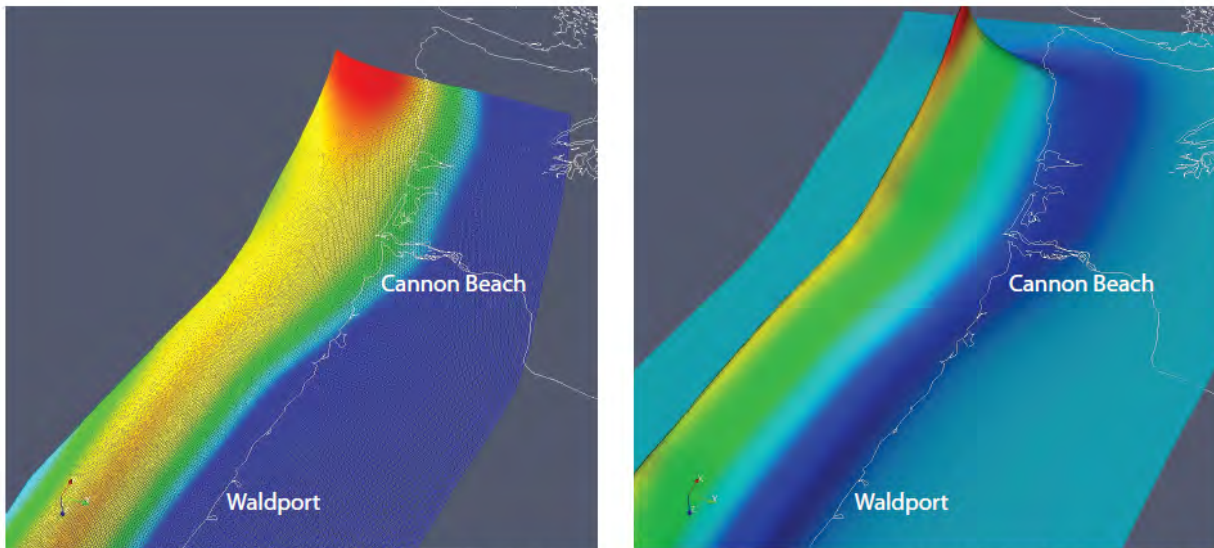


Figure A6. Fault slip distribution (left) and resultant surface vertical deformation (right) for the splay-fault model of medium p2a patch with symmetric fb76 slip distribution using 500 years of plate convergence to simulate coseismic slip. Red is ~17-18 m slip (left) and ~6 m uplift (right).

Figure 6-5. Comparison of two slip-deformation models for Cascadia tsunami generation.

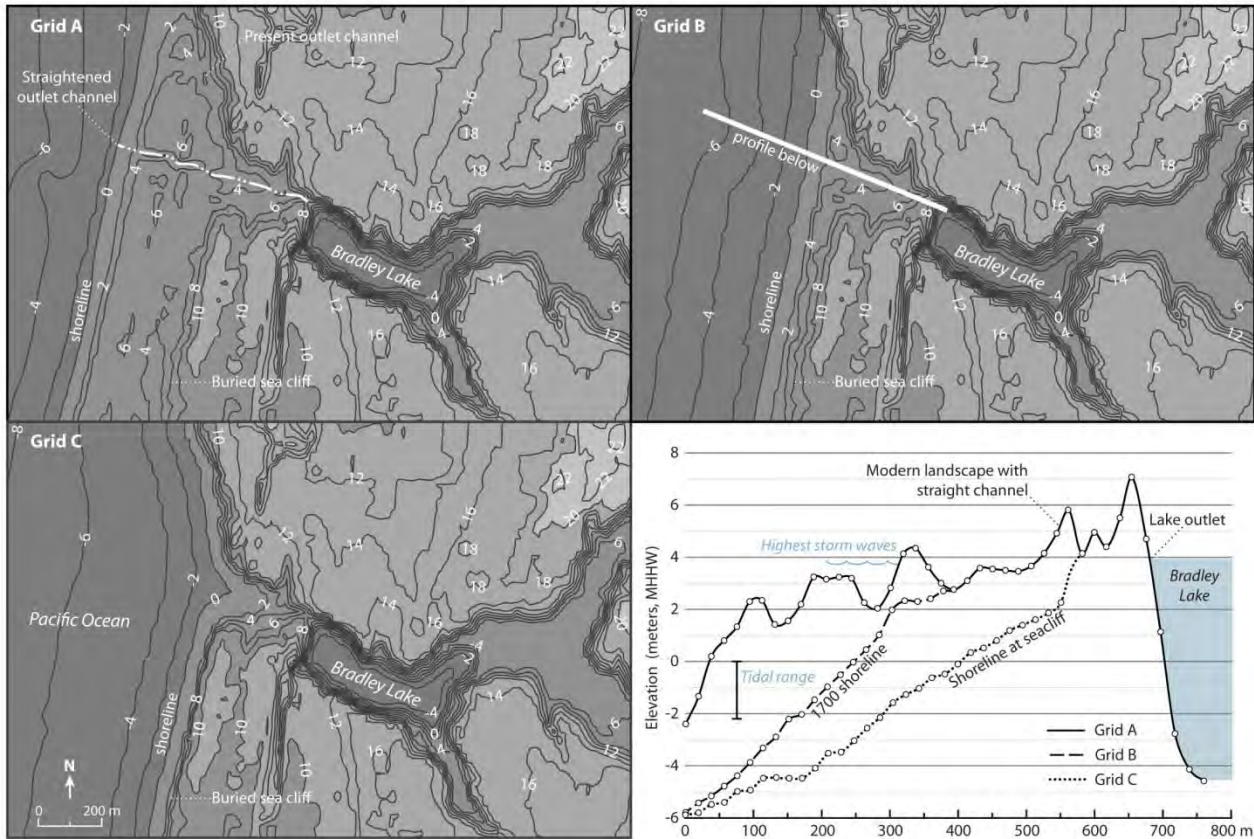


Table 1. Cascadia earthquake scenario parameters that produce tsunami inundation in Bradley Lake.

Fault slip distribution	Length (km)	Width (km) ^a	Recurrence interval (years)	Max. slip (m)	Slip at lake (m) ^b	Mean slip (m)	M_0 (10^{22} N m) ^c	Moment magnitude (M_w) ^d
<i>Modern Topography, Straight Outlet Channel (Grid A) —MSL+0.5</i>								
Symmetric slip	1100	105	500	20	16	10	4.5	9.0
Seaward-skewed slip ^e	1100	105	600	24	19	12	5.4	9.1
Slip diverted to splay fault	1100	83	460	18	15	9	3.3	8.9
<i>Circa 1925 shoreline (Grid B) —MSL+0.5</i>								
Symmetric slip	1100	105	400	16	13	8	3.6	9.0
Slip diverted to splay fault	1100	83	360	14	12	7	2.6	8.9
<i>Shoreline near seacliff (Grid C)—MSL+0.5</i>								
Symmetric slip	1100	105	290	11	9	6	2.6	8.9
Slip diverted to splay fault	1100	83	260	10	8	5	1.8	8.8
<i>Shoreline near seacliff (Grid C)—MHHW</i>								
Symmetric slip	1100	105	270	11	9	5	2.4	8.9
Slip diverted to splay fault	1100	83	250	10	8	5	1.8	8.8

Notes: Tidal elevation used in simulations, Mean Sea Level (MSL) + 0.5 m (1.55 m NAVD 88), approximates hindcast tide in AD 1700 (ref Mofjeld et al., 1997). Runs completed with grids A and B use MSL + 0.5 m tide; runs completed with grid C use MSL + 0.5 m and mean higher high water (MHHW, 2.07 m NAVD 88) tides.

^aEquivalent width for entire fault; actual width at latitude of Bradley Lake is smaller.

^bSlip estimates are the product of the recurrence interval times the convergence rate at latitude of Bradley Lake (32 mm yr⁻¹). Maximum slip estimates use a convergence rate close to 40 mm yr⁻¹.

Figure 6-6. Figure 6-3. Figure from in preparation paper by Rob Witter, Yinglong J Zhang, Kelin Wang, Chris Goldfinger, George R Priest and Jonathan C Allan, please do not reproduce or cite. Topographies modeled and minimum events require for each topography to get wave into lake.

The final results of the modeling for Bandon are shown in Figure 6-7, with progressively cooler colors representing the inundation from larger (and less likely) events. Arrival times for the peak waves are about 20 minutes, with runup locally as high as 25m. Just as important as the modeled runup is the modeled velocity, shown in insets in Figure 6-7. To put these values in perspective, the water depth/velocity combinations needed to knock over an adult are; 1m deep at 1.15m/sec, 60 cm deep at 1.75 m/sec and 30 cm deep at 3 m/sec.

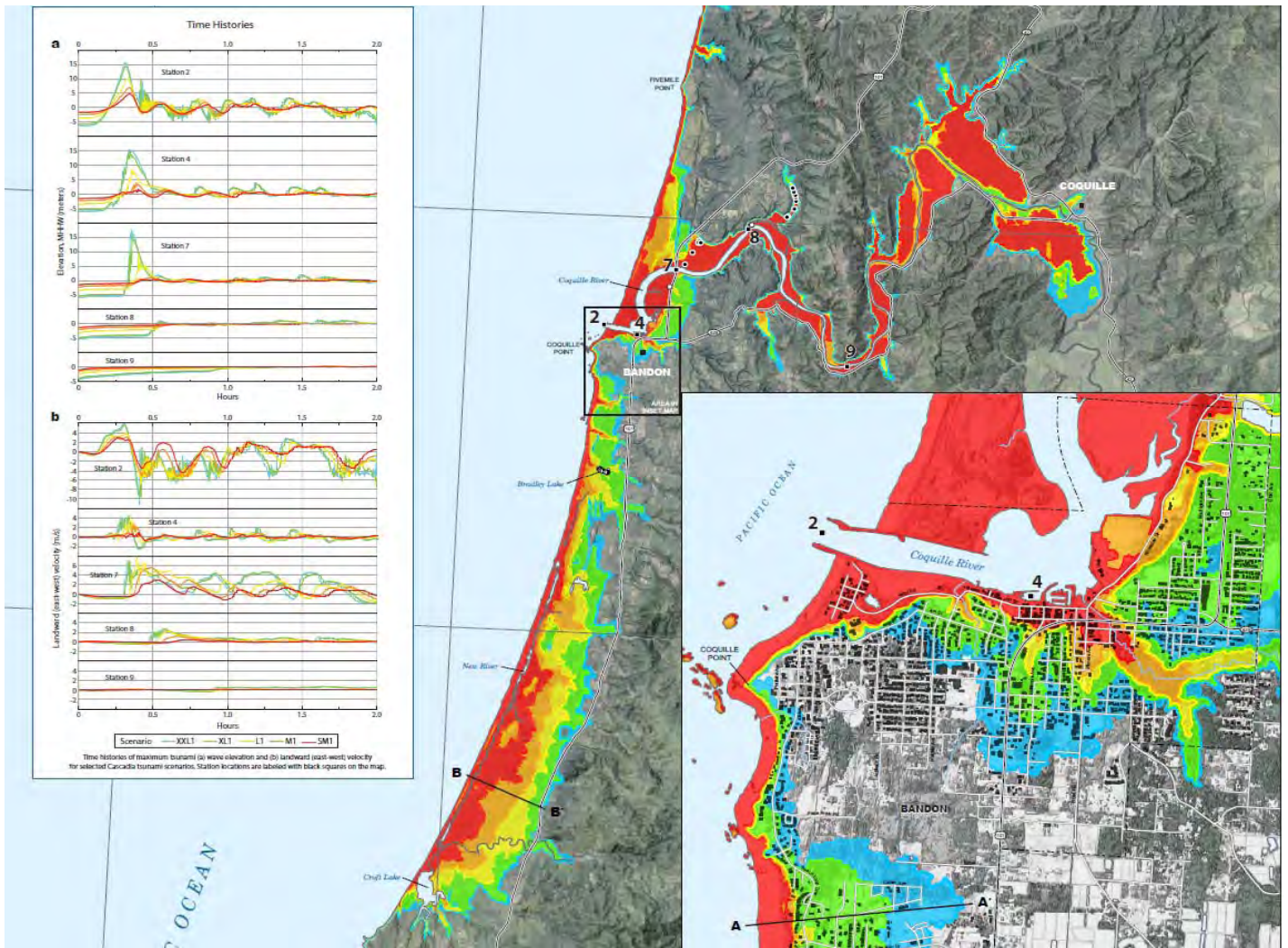


Figure 6-7. Bandon inundation models.